

1 Assessment of Simulated Soil Moisture from WRF Noah, Noah-MP, 2 and CLM Land Surface Schemes for Landslide Hazard Application

3 Lu Zhuo¹, Qiang Dai^{1,2*}, Dawei Han¹, Ningsheng Chen³, Binru Zhao^{1,4}

4 ¹WEMRC, Department of Civil Engineering, University of Bristol, Bristol, UK

5 ²Key Laboratory of VGE of Ministry of Education, Nanjing Normal University, Nanjing, China

6 ³The Institute of Mountain Hazards and Environment (IMHE), China

7 ⁴College of Water Conservancy and Hydropower Engineering, Hohai University, Nanjing, China

8 *Correspondence: civengwater@gmail.com

9 Abstract

10 This study assesses the usability of Weather Research and Forecasting (WRF) model simulated
11 soil moisture for landslide monitoring in the Emilia Romagna region, northern Italy during the 10-
12 year period between 2006 and 2015. Particularly three advanced Land Surface Model (LSM)
13 schemes (i.e., Noah, Noah-MP and CLM4) integrated with the WRF are used to provide
14 comprehensive detailed multi-layer soil moisture information. Through the temporal evaluation
15 with the single-point in-situ soil moisture observations, Noah-MP is the only scheme that is able
16 to simulate the large soil drying phenomenon close to the observations during the dry season, and
17 it also has the highest correlation coefficient and the lowest *RMSE* at most soil layers. The
18 evaluation of the WRF rainfall estimation shows there is no distinct difference among the three
19 LSMs, and their performances are in line with a published study for the central USA. Each
20 simulated soil moisture product from the three LSM schemes is then used to build a landslide
21 threshold prediction model, and within each model, 17 different exceedance probably levels from
22 1% to 50% are adopted to determine the optimal threshold scenario (in total there are 612
23 scenarios). Slope degree information is also used to separate the study region into different groups.
24 The threshold evaluation performance is based on the landslide forecasting accuracy using 45
25 selected rainfall events between 2014-2015. Contingency tables, statistical indicators, and

26 Receiver Operating Characteristic analysis for different threshold scenarios are explored. The
27 results have shown that, ~~the slope information is very useful in identifying threshold differences,~~
28 ~~with the threshold becoming smaller for the steeper area.~~ For landslide monitoring, Noah-MP at
29 the surface soil layer with 30% exceedance probability provides the best landslide monitoring
30 performance, with its hitting rate at 0.769, and its false alarm rate at 0.289.

31 **Keywords:** Emilia Romagna, Weather Research and Forecasting (WRF) Model, Land Surface
32 Model (LSM), Numerical Weather Prediction (NWP) model, landslide hazards, soil moisture.

33 1. Introduction

34 Landslide is a repeated geological hazard during rainfall seasons, which causes massive
35 destructions, loss of lives, and economic damages worldwide (Klose et al., 2014). ~~It is estimated~~
36 ~~between 2004 and 2016, there is a total number of 4862 fatal non-seismic landslides occurred~~
37 ~~around the world, which had resulted in the death of over 55,000 people (Froude and Petley, 2018).~~
38 ~~Those numbers are expected to further increase due to extreme events induced by climate changes~~
39 ~~and pressures of population expanding towards unstable hillside areas (Gariano and Guzzetti,~~
40 ~~2016;Petley, 2012).~~ The accurate predicting and monitoring of the spatiotemporal occurrence of
41 the landslide is the key to prevent/ reduce casualties and damages to properties and infrastructures.
42 ~~The~~ One of the most widely adopted methods s for ~~real-time~~ landslide monitoring-prediction is based
43 on ~~the simple empirical~~ rainfall threshold ~~rainfall threshold~~, ~~which has been used in many countries~~
44 ~~for their national landslide early warning system (Caine, 1980).~~ which ~~The method commonly~~
45 relies on building the rainfall intensity-duration curve using the information from the past landslide
46 events (Chae et al., 2017). However, such a method in many cases is insufficient for landslide
47 hazard assessment (Posner and Georgakakos, 2015), because in addition to rainfall, initial soil
48 moisture condition is one of the main triggering factors of the events (Glade et al., 2000;Crozier,

49 1999;Tsai and Chen, 2010;Hawke and McConchie, 2011;Bittelli et al., 2012;Segoni et al.,
50 2018b;Valenzuela et al., 2018;Bogaard and Greco, 2018).

51 ~~Although some researches have recognised the significance of soil moisture information for~~
52 ~~landslide early warning, most of them only rely on the antecedent precipitation index which simply~~
53 ~~depends on the amount of total rainfall accumulated before a landslide event occurs (Chleborad,~~
54 ~~2003;Calvello et al., 2015;Zêzere et al., 2005). Such a method is not recommended by several~~
55 ~~studies (Pelletier et al., 1997;Baum and Godt, 2010;Brocca et al., 2008), because during wet~~
56 ~~seasons, soil is often already saturated, and any additional rainfall falls on the earth surface will~~
57 ~~become direct runoff (Zhuo and Han, 2016b, a). As a result, the antecedent precipitation method~~
58 ~~can sometimes significantly overestimate the soil wetness condition. On the other hand,~~
59 ~~evapotranspiration is another factor which controls the soil moisture temporal evolution, which~~
60 ~~can also influence the relationship between the actual and the estimated soil moisture. Therefore,~~
61 ~~it is important that the landslide hazard assessment should be based on the real soil moisture~~
62 ~~information.~~

63 ~~Soil moisture varies largely both spatially and temporally (Zhuo et al., 2015b). For landslide~~
64 ~~applications, one potential soil moisture estimation method is through to accurately monitor soil~~
65 ~~moisture fluctuations in a critical zone (normally in remote regions), a dense network of soil~~
66 ~~moisture sensors is prerequisite. However, because of the complex installation and high~~
67 ~~maintenance fee especially in steep mountainous areas, such networks are normally unavailable.~~
68 ~~Several studies have found the usefulness of ground-measured soil moisture data for landslide~~
69 ~~monitoring purpose (Greco et al., 2010;Baum and Godt, 2010;Harris et al., 2012;Hawke and~~
70 ~~McConchie, 2011). However, due to the sparse distribution/no existence of in situ sensors in most~~
71 ~~hazardous regions, alternative soil moisture data sources need to be explored. One of the data~~

72 ~~sources is through~~ satellite remote sensing technologies. Although such technologies have been
73 improved significantly over the past decade, their retrieving accuracy is still largely affected by
74 ~~meteorological conditions (cloud coverage and rainfall),~~ frozen soil conditions (Zhuo et al.,
75 2015a), and dense vegetation coverages particularly in mountainous regions (Temimi et al., 2010);
76 furthermore, the acquired data only covers the top few centimetres of soil. Although the more
77 recently launched satellites such as Sentinel-1 (1 km, and 3 days resolution) has shown some
78 promising performance of soil moisture estimation, their coverage period availability only
79 covers the recent years is currently limited (since, and their resolution is too low (e.g., 0.25 degree)
80 for detailed regional studies (Zhuo et al., 2016). Those disadvantages restrict the full utilisation of
81 satellite soil moisture products for landslide monitoring application as discussed in our previous
82 study (Zhuo et al., 2019). In (Zhuo et al., 2019), it is discussed that both the temporal and spatial
83 resolutions of the ESA CCI satellite soil moisture product (Dorigo et al., 2017) is too coarse for
84 landslide applications, and its data is mostly only available after the year 2002. Moreover
85 the shallow depth soil moisture observation from the satellite hinders the accuracy of landslide
86 predictions. Therefore, other alternative soil moisture estimation methods need to be
87 explored.

88 One emerging area relies on modelling. Some studies have used modelled soil moisture data for
89 landslide applications (Ponziani et al., 2012; Ciabatta et al., 2016; Zhao et al., 2019a; Zhao et al.,
90 2019b). However, to our knowledge, there is a lack of existing study using ~~Another soil moisture~~
91 ~~data source~~ One emerging area relies on the state-of-the-art Land Surface Models (LSMs) modelled
92 soil moisture for landslide studies, such as the Noah LSM (Ek et al., 2003) and the Community
93 Land Model (CLM) (Oleson et al., 2010). LSMs describe the interactions between the atmosphere
94 and the land surface by simulating exchanges of momentum, heat and water within the Earth

95 system (Maheu et al., 2018). They are capable of simulating the most important subsurface
96 hydrological processes (e.g., soil moisture) and can be integrated with the advanced Numerical
97 Weather Prediction (NWP) system like WRF (Weather Research and Forecasting) (Skamarock et
98 al., 2008) for comprehensive soil moisture estimations (i.e., through the surface energy balance,
99 the surface layer stability and the water balance equations) (Greve et al., 2013). NWP-based (i.e.,
100 with integrated LSM, thereafter) soil moisture estimations have many advantages, for instance
101 their spatial and temporal resolution can be set at different scales depending on the input
102 datasets discretionarily to fit different various application requirements; their coverage is global,
103 and the estimated soil moisture data covers multiple soil layers (from the shallow surface layer to
104 deep root-zones); as well as a number of globally-covered data products can provide the necessary
105 boundary and initial conditions for running the models. Soil moisture estimated through such an
106 approach has been widely recognised and demonstrated in many studies, which cover a broad
107 range of applications from hydrological modelling (Srivastava et al., 2013a;Srivastava et al., 2015),
108 drought studies (Zaitchik et al., 2013), flood investigations (Leung and Qian, 2009), to regional
109 weather prediction (Stéfanon et al., 2014). Therefore, NWP-based soil moisture datasets could
110 provide valuable information for landslide applications. However, to our knowledge, relevant
111 research has never been carried out.

112 The aim of this study hence is to evaluate the usefulness of NWP modelled soil moisture for
113 landslide monitoring. Here the advanced WRF model (version 3.8) is adopted, because it offers
114 numerous physics options such as micro-physics, surface physics, atmospheric radiation physics,
115 and planetary boundary layer physics (Srivastava et al., 2015), and can integrate with a number of
116 LSM schemes, each varying in physical parameterisation complexities. So far there is limited
117 literature in comparing the soil moisture accuracy of different LSMs options in the WRF model.

118 Therefore, in this study, we select three of the WRF's most advanced LSM schemes (i.e., Noah,
119 Noah-Multiparameterization (Noah-MP), and CLM4) to compare their soil moisture performance
120 for landslide hazard assessment. Furthermore, since all the three schemes can provide multi-layer
121 soil moisture information, it is useful to include all those simulations for the comparison so that
122 the optimal depth of soil moisture could be determined for the landslide monitoring application.

123 ~~The large physiographic variability, plus the abundance of the historical landslide events data,~~
124 ~~makes Italy a good place for this research.~~In order to compare with the performance of our previous
125 study on using the satellite soil moisture data (Zhuo et al., 2019), ~~the same study area~~ ~~Here an~~
126 ~~Italian region~~ called Emilia Romagna is used here~~selected~~. The study period covers 10 years from
127 2006 to 2015 to include a long-term record of landslide events. In addition, because slope angle is
128 one of the major factors s controlling the stability of the slope, it is hence used in this study to
129 divide the study area into several slope groups, so that a more accurate ~~threshold-landslide~~
130 prediction model could be built.

131 The description of the study area and the used datasets are included in Section 2. Methodologies
132 regarding the WRF model, the related LSM schemes and the adopted landslide threshold
133 evaluation approach are provided in Section 3. Section 4 shows the WRF soil moisture evaluation
134 results against the in-situ observations, and the WRF rainfall evaluations over the whole study area.
135 Section 5 covers the comparison results of the WRF modelled soil moisture products for landslide
136 applications. The discussion and conclusion of the study are included in Section 6.

137 2. Study Area and Datasets

138 2.1 Study Area

139 The study area is in the Emilia Romagna Region, northern Italy (Figure 1). Its population density
140 is high. The region has high mountainous areas in the S-SW, and wide plain areas towards NE,
141 with a large elevation difference (i.e., 0 m to 2125 m) across 50 km distance from the north to the
142 south (Rossi et al., 2010). The region has a mild Mediterranean climate with distinct wet and dry
143 seasons (i.e., dry season between May and October, and wet season between November and April).
144 The study area tends to be affected by landslide events easily, with approximately one-fifth of the
145 mountainous zone covered by active or dormant landslide deposits (Bertolini et al., 2005). Rainfall
146 is by far the primary triggering factor of landslides in the region, followed by snow melting:
147 shallow landslides are mainly triggered by short but exceptionally intense rainfall, and long and
148 moderate rainfall events over saturated conditions, while deep-seated landslides have a more
149 complex response to rainfall and are mainly caused by moderate but exceptionally prolonged (even
150 up to 6 months) periods of rainfalls (Segoni et al., 2015). Due to the abundant data available in the
151 region, several studies on regional scale landslide prediction and early warning have been
152 published (Berti et al., 2012; Martelloni et al., 2012; Lagomarsino et al., 2015; Segoni et al.,
153 2018b; Segoni et al., 2018a; Lagomarsino et al., 2013). Interested readers can refer to those studies
154 for more information.

155 **2.2 Selection of The Landslide Events**

156 The landslides catalog is collected from the Emilia Romagna Geological Survey (Berti et al., 2012).
157 The information included in the catalog are: location, date of occurrence, the uncertainty of date,
158 landslide characteristics (dimensions, type, and material), triggering factors, damages, casualties,
159 and references. Unfortunately, many pieces of the information ~~are~~ are missing from the records in
160 many cases. In order to organise the data in a more systematic way so that only the relevant events
161 are retained, a two-step event selection procedure is initially carried out based on: 1) rainfall-

162 induced only; and 2) high spatial-temporal accuracy (exact date and coordinates). Finally, a
163 revision of the information about the type of slope instabilities such as landslide/debris
164 flow/rockfall and the characteristics of the affected slope (natural or artificial) is also carried out
165 over the selected records (Valenzuela et al., 2018). The catalog period used in this study covers
166 between 2006 and 2015, which is in accordance with the WRF² model run. After filtering the data
167 records, only one-fifths of them (i.e., 157 events) is retained. The retained events are shown as
168 single circles in Figure 2, with slope information (calculated through the Digital Elevation Model
169 (DEM) data) also presented in the background. It can be seen the spatial distribution of the
170 occurred landslide events is very heterogeneous, with nearly all of them occurred in the hilly
171 regions. ~~During the study period, the regional landslide occurrence is mainly dominated by the
172 spatial distribution of the weak earth units and the critical rainfall periods.~~

173 2.3 Datasets

174 There is a total of 19 soil moisture stations available within the study area, however, based on our
175 collected data, only one of them at the San Pietro Capofiume (latitude 44° 39' 13.59", longitude
176 11° 37' 21.6") provides long-term valid soil moisture retrievals (i.e., 2006 to 2017). WWe have
177 checked the data from all the rest of the stations, they are either absent (or have very big data gaps)
178 or do not cover the research period at all. Therefore, only the San Pietro Capofiume station is used
179 for the WRF soil moisture temporal evaluation. The soil moisture is measured from 10 cm to 180
180 cm deep in the soil at 5 depths, by the Time Domain Reflectometry (TDR) instrument. Data is
181 recorded in the unit of volumetric water content (m^3/m^3) and at daily timestep (Pistocchi et al.,
182 2008). The data used in this study is between 2006 and 2015. Rainfall data over the whole study
183 area is collected from over 200 tipping-bucket rain gauges, which are used to assess the quality of
184 the WRF model's rainfall estimations in the study area, as well as for rainfall events selection

185 ~~during the In order to select rainfall events for~~ Year 2014 and 2015, ~~data from 200 tipping-bucket~~
186 ~~rain gauges are collected and analysed within the region.~~

187 To drive a NWP model like WRF for soil moisture simulations, several globally-coved data
188 products can be chosen for extracting the boundary and initial conditions information, for instance,
189 the European Centre for Medium-Range Weather Forecasts (ECMWF) reanalysis (ERA-Interim)
190 and the National Centre for Environmental Prediction (NCEP) reanalysis are two of the most
191 commonly used data products. It has been found by (Srivastava et al., 2013b) that the ERA-Interim
192 datasets can provide better boundary conditions than the NCEP datasets for WRF hydro-
193 meteorological predictions in Europe, which is therefore adopted in this study to drive the WRF
194 model. The spatial resolution of the ERA-Interim is approximately 80 km. The data is available
195 from 1979 to present, containing 6-hourly gridded estimates of three-dimensional meteorological
196 variables, and 3-hourly estimates of a large number of surface parameters and other two-
197 dimensional fields. A comprehensive description of the ERA-Interim datasets can be found in (Dee
198 et al., 2011)

199 The Shuttle Radar Topography Mission (SRTM) 3 Arc-Second Global (~ 90m) DEM datasets ~~is~~
200 ~~are~~ downloaded and used as the basis for the slope degree calculations. SRTM DEM data has been
201 widely used for ~~elevation-elevation~~-related studies worldwide due to its high quality, near-global
202 coverage, and free availability (Berry et al., 2007).

203 **3. Methodologies**

204 **3.1 WRF Model and The Three Land Surface Model Schemes**

205 The WRF model is a next-generation, non-hydrostatic mesoscale NWP system designed for both
206 atmospheric research and operational forecasting applications (Skamarock et al., 2005). The model

207 is powerful enough in modelling a broad range of meteorological applications varying from tens
208 of metres to thousands of kilometres (NCAR, 2018). It has two dynamical solvers: the ARW
209 (Advanced Research WRF) core and the NMM (Nonhydrostatic Mesoscale Model) core. The
210 former has more complex dynamic and physics settings than the latter which only has limited
211 setting choices. Hence in this study WRF with ARW dynamic core (version 3.8) is used to perform
212 all the soil moisture simulations.

213 The main task of LSM within the WRF is to integrate information generated through the surface
214 layer scheme, the radiative forcing from the radiation scheme, the precipitation forcing from the
215 microphysics and convective schemes, and the land surface conditions to simulate the water and
216 energy fluxes (Ek et al., 2003). WRF provides several LSM options, among which three of them
217 are selected in this study as mentioned in the introduction: Noah, Noah-MP, and CLM4. Table 1
218 gives a simple comparison of the three models. The detailed description of the models is written
219 below in the order of increasing complexity in regards of the way they deal with thermal and
220 moisture fluxes in various layers of soil, and their vegetation, root and canopy effects
221 (Skamarock et al., 2008).

222 **3.1.1 Noah**

223 Noah is the most basic amongst the three selected LSMs. It is one of the ‘second generation’ LSMs
224 that relies on both soil and vegetation processes for water budgets and surface energy closures
225 (Wei et al., 2010). The model is capable of modelling soil and land surface temperature, snow
226 water equivalent, as well as the general water and energy fluxes. The model includes four soil
227 layers that reach a total depth of 2 m in which soil moisture is calculated. Its bulk layer of canopy
228 -snow-soil (i.e., lack the abilities in simulating photosynthetically active radiation (PAR),
229 vegetation temperature, correlated energy, and water, heat and carbon fluxes), ‘leaky’ bottom (i.e.,

230 drained water is removed immediately from the bottom of the soil column which can result in
231 much fewer memories of antecedent weather and climate fluctuations) and simple snow melt-thaw
232 dynamics are seen as the model's demerits (Wharton et al., 2013). Noah calculates the soil moisture
233 from the diffusive form of Richard's equation for each of the soil layer (Greve et al., 2013), and
234 the evapotranspiration from the Ball-Berry equation (considering both the water flow mechanism
235 within soil column and vegetation, as well as the physiology of photosynthesis (Wharton et al.,
236 2013)).

237 **3.1.2 Noah-MP**

238 Noah-MP (Niu et al., 2011) is an improved version of the Noah LSM, in the aspect of better
239 representations of terrestrial biophysical and hydrological processes. Major physical mechanism
240 improvements directly relevant to soil water simulations include: 1) introducing a more permeable
241 frozen soil by separating permeable and impermeable fractions (Cai, 2015), 2) adding an
242 unconfined aquifer immediately beneath the bottom of the soil column to allow the exchange of
243 water between them (Liang et al., 2003), and 3) the adoption of a TOPMODEL (TOPography
244 based hydrological MODEL)-based runoff scheme (Niu et al., 2005) and a simple SIMGM
245 groundwater model (Niu et al., 2007) which are both important in improving the modelling of soil
246 hydrology. Noah-MP is unique compared with the other LSMs, as it is capable of generating
247 thousands of parameterisation schemes through the different combinations of "dynamic leaf,
248 canopy stomatal resistance, runoff and groundwater, a soil moisture factor controlling stomatal
249 resistance (the β factor), and six other processes" (Cai, 2015). The scheme option used in the study
250 are: Ball-Berry scheme for canopy stomatal resistance, Monin-Obukhov scheme for surface layer
251 drag coefficient calculation, the Noah based soil moisture factor for stomatal resistance, the
252 TOPMODEL runoff with the SIMGM groundwater, the linear effect scheme for soil permeability,

253 the two-stream applied to vegetated fraction scheme for radiative transfer, the CLASS (Canadian
254 Land Surface Scheme) scheme for ground surface albedo option, and the Jordan (Jordan, 1991)
255 scheme for partitioning precipitation between snow and rain.

256 **3.1.3. CLM4**

257 CLM4 is developed by the National Center for Atmospheric Research (NCAR) to serve as the land
258 component of its Community Earth System Model (formerly known as the Community Climate
259 System Model) (Lawrence et al., 2012). It is a ‘third generation’ model that incorporates the
260 interactions of both nitrogen and carbon in the calculations of water and energy fluxes. Compared
261 with its previous versions, CLM4 (Oleson et al., 2008) has multiple enhancements relevant to soil
262 moisture computing. For instance, the model’s soil moisture is estimated by adopting an improved
263 one-dimensional Richards equation (Zeng and Decker, 2009); the new version allows the dynamic
264 interchanges of soil water and groundwater through an improved definition of the soil column’s
265 lower boundary condition that is similar to the Noah-MP’s (Niu et al., 2007). Furthermore, the
266 thermal and hydrologic properties of organic soil are included for the modelling which is based on
267 the method developed in (Lawrence and Slater, 2008). The total ground column is extended to 42
268 m depth, consisting 10 soil layers unevenly spaced between the top layer (0.0–1.8 cm) and the
269 bottom layers (229.6–380.2 cm), and 5 bedrock layers to the bottom of the ground column
270 (Lawrence et al., 2011). Soil moisture is estimated for each soil layer.

271 **3.2 WRF Model Parameterization**

272 The WRF model is centred over the Emilia Romagna Region with three nested domains (D1, D2,
273 D3 with the horizontal grid sizes of 45 km, 15 km, and 5 km, respectively), of which the innermost
274 domain (D3, with 88 x 52 grids (west-east and south-north, respectively)) is used in this study. A

275 two-way nesting scheme is adopted allowing information from the child domain to be fed back to
276 the parent domain. With atmospheric forcing, static inputs (e.g., soil and vegetation types), and
277 parameters, the WRF model needs to be spunspin-up to reach its equilibrium state before it can be
278 used (Cai et al., 2014;Cai, 2015). In this study, WRF is spunspin-up by running through the whole
279 year of 2005. After the spin-up, the WRF model for each of the selected LSM scheme is executed
280 in daily timestep from January 1, 2006, to December 31, 2015, using the ERA-Interim datasets.

281 The microphysics scheme plays a vital role in simulating accurate rainfall information which in
282 turn is important for modelling the accurate soil moisture variations. WRF V3.8 is supporting 23
283 microphysics options range from simple to more sophisticated mixed-phase physical options. In
284 this study, the WRF Single-Moment 6-class scheme is adopted which considers ice, snow and
285 graupel processes and is suitable for high-resolution applications (Zaidi and Gisen, 2018). The
286 physical options used in the WRF setup are Dudhia shortwave radiation (Dudhia, 1989) and Rapid
287 Radiative Transfer Model (RRTM) longwave radiation (Mlawer et al., 1997). Cumulus
288 parameterization is based on the Kain-Fritsch scheme (Kain, 2004) which is capable of
289 representing sub-grid scale features of the updraft and rain processes, and such a capability is
290 beneficial for real-time modelling (Gilliland and Rowe, 2007). The surface layer parameterization
291 is based on the Revised fifth-generation Pennsylvania State University–National Center for
292 Atmospheric Research Mesoscale Model (MM5) Monin-Obukhov scheme (Jiménez et al., 2012).
293 The Yonsei University scheme (Hong et al., 2006) is selected to calculate the planetary boundary
294 layer. The parameterization schemes used in the WRF modelling are shown in Table 2. The
295 datasets for land use and soil texture are available in the pre-processing package of WRF. In this
296 study, the land use categorisation is interpolated from the MODIS 21-category data classified by

297 the International Geosphere Biosphere Programme (IGBP). The soil texture data are based on the
298 Food and Agriculture Organization of the United Nations Global 5-minutes soil database.

299 **3.3 Translation of Observed and Simulated Soil Moisture Data to Common Soil Layers**

300 Since all soil moisture datasets have different soil depths, it is difficult for a direct comparison.
301 The Noah and Noah-MP models include four soil layers, centred at 5, 25, 70, and 150 cm,
302 respectively. Whereas CLM4 model has 10 soil layers, centered at 0.9, 3.2, 6.85, 12.85, 22.8, 39.2,
303 66.2, 110.65, 183.95, 304.9 cm, respectively. Moreover, the in-situ sensor measures soil moisture
304 centred at 10, 25, 70, 135, and 180 cm. In order to ~~tackle the inconsistency issue of soil depths~~
305 make the datasets comparable at consistent soil depths, the simple linear interpolation approach
306 described in (Zhuo et al., 2015b) is applied in this study, and a benchmark of the soil layer centred
307 at 10, 25, 70 and 150 cm is adopted.

308 **3.4 Soil Moisture Thresholds Build Up and Evaluations**

309 To build and evaluate the soil moisture thresholds for landslides forecasting, all datasets have been
310 grouped into two portions: 2006-2013 for the establishment of thresholds, and 2014-2015 for the
311 evaluation. The determination of soil moisture thresholds is based on determining the most suitable
312 soil moisture triggering level for landslides occurrence by trying a range of exceedance
313 probabilities (percentiles). For example, a 10% exceedance probability is calculated by
314 determining the 10% percentile result of the soil moisture datasets that ~~is~~are related to the occurred
315 landslides. The exceedance probability method is commonly utilised in landslide early warning
316 studies for calculating the rainfall-thresholds, which is therefore adopted here to examine its
317 performance for soil moisture threshold calculations.

318 To carry out the threshold evaluation, 45 rainfall events (during 2014-2015) are selected for the
319 purpose. The rainfall events are separated based on at least one-day of dry period (i.e., a period
320 without rainfall) (Dai et al., 2014; Dai et al., 2015; Dai et al., 2016). The rainfall data from each rain
321 gauge station is firstly combined using the Thiessen Polygon method, and with visual analysis, the
322 45 events are then finally selected. The information about the selected rainfall events can be found
323 in Section 5. The threshold evaluation is based on the statistical approach described in (Gariano et
324 al., 2015; Zhuo et al., 2019), where soil moisture threshold can be treated as a binary classifier of
325 the soil moisture conditions that are likely or unlikely to cause landslide events. With this
326 hypothesis, the likelihood of a landslide event can either be *true (T)* or *false (F)*, and the threshold
327 forecasting can either be *positive (P)* or *negative (N)*. The combinations of those four conditions
328 can lead to four statistical outcomes (Figure 3a) that are: *true positive (TP)*, *true negative (TN)*,
329 *false positive (FP)*, and *false negative (FN)* (Wilks, 2011). ~~The detailed description of each~~
330 ~~outcome is covered in~~ (Zhuo et al., 2019). Using the four outcomes, two statistical scores can be
331 determined.

332 The Hit Rate (*HR*), which is the rate of the events that are correctly forecasted. Its formula is:

$$333 \quad HR = \frac{TP}{TP+FN} \quad (1)$$

334 in the range of 0 and 1, with the best result as 1.

335 The False Alarm Rate (*FAR*), which is the rate of false alarms when the event did not occur. Its
336 formula is:

$$337 \quad FAR = \frac{FP}{FP+TN} \quad (2)$$

338 in the range of 0 and 1, with the best result as 0.

339 For any soil moisture product, each threshold calculated ~~for each of the slope degree group~~ is
340 adopted to determine *T*, *F*, *P*, and *N*, respectively. Those values are finally integrated to find the
341 overall scores of *TP*, *FN*, *FP*, *TN*, *HR*, and *FAR*. The threshold performance is then judged via the

342 Receiver Operating Characteristic (ROC) analysis (Hosmer and Lemeshow, 1989;Fawcett, 2006).
343 As shown in Figure 3b, ROC curve is based on *HR* against *FAR*, and each point in the curve
344 represents a threshold scenario (i.e., selected exceedance probabilities). The optimal result (the red
345 point) can only be realised when the *HR* reaches 1 and the *FAR* reduces to 0. The closer the point
346 to the red point, the better the forecasting result is. To analyse and compare the forecasting
347 performance numerically, the Euclidean distances (d) for each scenario to the optimal point are
348 computed.

349 **4. WRF Soil Moisture Analysis and Model Evaluations**

350 In this study, the evaluation is based on the daily mean soil moisture. The reason for not using the
351 antecedent soil moisture condition plus rainfall data on the day is because the purpose of this study
352 is to explore the relationship between different WRF simulated soil moisture and landslides solely.
353 In general, soil moisture is a predisposing factor for slope instability, while rainfall is the triggering
354 factor. The same rainfall may trigger or not a landslide depending on the soil moisture content at
355 the time of the rainfall event. The mean soil moisture on the day of the landslide implicitly account
356 for both the initial soil moisture and the effective rainfall absorbed by the ground, and can be a
357 robust indicator of the hydrological condition of the slope.

358 **3.34.1 Soil Moisture Temporal Comparisons**

359 Although there is only one soil moisture sensor that provides long-term soil moisture data in the
360 study region, it is still useful to compare it with the WRF estimated soil moisture. Particularly, it
361 has been shown that soil moisture measured at a site location can reflect the temporal fluctuations
362 of soil moisture for its surrounding region, up to 500 km in radius (Entin et al., 2000). With the
363 WRF's relatively high resolution of 5 km, the temporal comparison with the in-situ observations

364 ~~should provide some meaningful results.~~ In this study, we carry out a temporal comparison
365 between all the three WRF soil moisture products with the in-situ observations. The comparison
366 is implemented over the period from 2006 to 2015, and the WRF grid closest to the in-situ sensor
367 location is chosen. Figure 4 shows the comparison results at the four soil depths. The statistical
368 performance (correlation coefficient r and Root Mean Square Error $RMSE$) of the three LSM
369 schemes are summarised in Table 3. Based on the statistical results, Noah-MP surpasses other
370 schemes at most soil layers, except for Layer 2 where CLM4 shows stronger correlation and Layer
371 4 where Noah gives smaller $RMSE$ error. For Noah-MP, the best correlation is observed at the
372 surface layer (0.809), followed by the third (0.738), second (0.683) and fourth (0.498) layers; and
373 based on $RMSE$, the best performance is again observed at the surface layer and followed by the
374 second, third and fourth layers in sequence (as 0.060, 0.070, 0.088, and 0.092 m^3/m^3 , respectively).
375 From the temporal plots, it can be seen at all four soil layers, all three LSM schemes can produce
376 ~~the~~ soil moisture's seasonal cycle ~~very well~~ with most upward and downward trends successfully
377 represented. However, both the Noah and the CLM4 overestimate the variability at the upper two
378 soil layers during almost the whole study period, and the situation is the worst for the Noah.
379 Comparatively, the Noah-MP can ~~better~~ capture the wet soil moisture conditions ~~very well~~
380 especially at the surface layer; and it is the only model of the three that is able to simulate the large
381 soil drying phenomenon close to the observations during the dry season, except for some extremely
382 dry days. Towards 70 cm depth, although Noah-MP is still able to capture most of the soil moisture
383 variabilities during the drying period, it significantly underestimates soil moisture values for most
384 wet days. Similar underestimation results can be observed for CLM4 and Noah during the wet
385 season at 70 cm; furthermore, both schemes are again not capable of reproducing the extremely
386 drying phenomenon and overestimate soil moisture for most of the dry season days. It is surprising

387 to see that at the deep soil layer (150 cm), all soil moisture products are underestimated, in
388 particular, the outputs from the CLM4 and the Noah-MP only show small fluctuations. However,
389 the soil moisture measurements from the in-situ sensor also get our attention as they show strange
390 fluctuations with numerous sudden drops and rise situations observed. The strange phenomenon
391 is not expected at such a deep soil layer (although groundwater capillary forces can increase the
392 soil moisture, its rate is normally very slow). One possible reason we suspect is due to sensor
393 failure in the deep zone. Therefore, the assessment result for the deep soil layer should be
394 considered unreliable. Overall for the Noah-MP, in addition to producing the highest correlation
395 coefficient and the lowest *RMSE*, its simulated soil moisture variations are the closest to the
396 observations. The better performance of the Noah-MP over the other two models agrees with the
397 results found in (Cai et al., 2014) (note: the paper uses standalone models, which are not coupled
398 with WRF). Also, it has been discussed in (Yang et al., 2011), the Noah MP presents a clear
399 improvement over the Noah in simulating soil moisture globally. However, it is noted the
400 evaluation results are only based on one soil moisture sensor located at the plain part of the study
401 area.

402 4.2 Spatial Comparisons Rainfall Evaluations

403 Since soil moisture is related to rainfall, it is useful to carry out the evaluations of WRF rainfall
404 estimations against the observations in the study area. The spatial plot of *R* for the three LSMs is
405 shown in Figure 5. It can be seen the performance of the three models are very close to each other,
406 with only small differences over the whole study region. In general, the performance is the best in
407 the Southeast region, with *R* reaches above 0.70. The poorest performance is observed in the
408 Northeast region and some parts of the mountain zone. Based on the spatial distribution of *R*, there
409 is no clear correlation between the WRF rainfall performance and the topography of the region.

410 The boxplot for the R performance is illustrated in Figure 6a. It can be seen again the performances
411 of the three models are very similar. Generally, R ranges between around 0.10 and 0.80, and with
412 the majority of the region performs around 0.40. $RMSE$ performance is also calculated. Similar to
413 the results of R , it has been found the $RMSE$ spatial distributions are very similar among the three
414 models. Therefore, the $RMSE$ spatial distribution map is not included in this paper. The boxplot of
415 the $RMSE$ is shown in Figure 6b. Generally, the $RMSE$ ranges between around 4 mm and 12 mm,
416 with some outliers between around 12 mm and 20 mm. Majority of the region performs at around
417 7 mm $RMSE$. The statistical calculations are summarised in Table 4. Based on the results of R and
418 $RMSE$, the WRF rainfall estimation performance in Emilia is similar to the one found in central
419 USA (Van Den Broeke et al., 2018).

420 ~~Figure 5, 6 shows the spatial distribution of soil moisture simulations (via the three WRF LSM~~
421 ~~schemes) at the four soil layers on a typical day during the dry and the wet seasons, respectively.~~
422 ~~It is clear to see on the dry season day, Noah gives the wettest soil moisture simulation amongst~~
423 ~~the three schemes, followed by CLM4 and Noah-MP. The soil moisture spatial pattern of the three~~
424 ~~schemes more or less agrees with each, that is with wetter soil condition found in the central (in~~
425 ~~line with the location of the river mainstream) and South-West part of the study region and dryer~~
426 ~~soil condition in the Southern boundary and East part of the study region. On the wet season day,~~
427 ~~Noah again produces wetter soil moisture data than the other two schemes, and it shows a distinct~~
428 ~~wet patch at the Southern boundary while both the Noah-MP and the CLM4's simulations indicate~~
429 ~~that part as the driest of the whole region. The disagreement among the LSMs at the Southern~~
430 ~~boundary could be due to the particularly high elevation (above 2000 m) and snow existence at~~
431 ~~that region, and the three schemes use different theories to deal with such conditions. The~~
432 ~~improvement in the Noah-MP and the CLM4 is mainly attributed to the better simulation of snow,~~

433 ~~in particular, it has been found Noah-MP can better simulate the snowmelt phenomenon over the~~
434 ~~other two schemes (Cai et al., 2014), because it has better representations of ground heat flux,~~
435 ~~retention, percolation and refreezing of melted liquid water within the multilayer snowpack (Yang~~
436 ~~et al., 2011). Furthermore, it can be seen Noah-MP has a clear spatial pattern of the soil moisture~~
437 ~~in the region, that is with drier areas found near the river mainstream, and Southern boundary, and~~
438 ~~wetter zones in the North and the South. On the contrary, Noah and CLM4 simulated soil moisture~~
439 ~~show a relatively smaller difference spatially, especially for CLM4.~~

440 **5. The Assessment of WRF Soil Moisture Threshold for Landslide Monitoring**

441 As introduced at the beginning of the paper, previous works have demonstrated that in complex
442 geomorphologic settings (e.g., in Emilia Romagna), a rainfall threshold approach is too simple and
443 more hydrologically driven approaches need to be established. This section is to assess if the spatial
444 distribution of soil moisture can provide useful information for landslide monitoring at the regional
445 scale. Particularly, all three soil moisture products simulated through the WRF model are used to
446 derive threshold models, and the corresponding landslide prediction performances are then
447 compared statistically. Here the threshold is defined as the crucial soil moisture condition above
448 which landslides are likely to happen.

449 Among different factors for controlling the stability of slope, the slope angle is one of the most
450 critical ones. From the slope angle map in Figure 2, it can be seen the region has a clear spatial
451 pattern of high and low slope areas, with the majority of the high-slope areas (can be as steep as
452 around 40 degrees) located in the mountainous Southern part and the river valleys. Based on the
453 analysed events data, Moreover, there is an obvious causal relationship between the slope angle
454 and the landslide occurrence, as all the landslides happened during the study period are mainly
455 located in the high-slope region, with a particularly high concentration around the central Southern

456 part. The spatial distribution of the landslide events is also in line with the overall geological
457 characteristics of the region, i.e., the Southern part mainly constitutes outcrop of sandstone rocks
458 that make up the steep slopes and are covered by a thin layer of permeable sandy soil, which are
459 highly unstable (Zhuo et al., 2019). Therefore, instead of only using one soil moisture threshold
460 for the whole study area, it is useful to divide the region into several slope groups so that within
461 each group a threshold model is built. To derive soil moisture threshold individually under
462 different slope conditions, all data has been divided into three groups based on the slope angle
463 (0.4-1.86°; 1.87-9.61°; 9.52-40.43°; since no landslide events are recorded under the 0-0.39° group,
464 the group is not considered here), as results, all groups have equal coverage areas. There are
465 different ways to group the slopes. In this study, three groups have been defined with similar sizes
466 so that relatively reliable results could be achieved from the statistical point of view.

467 In order to find the optimal threshold so that there are least missing alarms (i.e., threshold is
468 overestimated) and false alarms (i.e., threshold is underestimated), we test out 17 different
469 exceedance probabilities from 1% to 50%. For each LSM scheme, the total number of threshold
470 models is 204, which is the resultant of different combinations of slope groups, soil layers, and
471 exceedance probability conditions. The calculated thresholds for all LSM schemes under three
472 slope groups are plotted in Figure 7. Overall there is a very-clear trend between the slope angle
473 and the soil moisture threshold, that is with threshold becoming smaller for steeper areas. The
474 correlation is particularly more evident at the upper three soil layers (i.e., the top 1 m depth of soil),
475 with only a few exceptions for Noah and CLM4 at the 1% and the 2% exceedance probabilities.
476 At the deep soil layer centred at 150 cm, the soil moisture threshold difference between Slope
477 Group (S.G.) 2 and 3 becomes very small for all the three LSM schemes. This could be partially
478 because at the deep soil layer, the change of soil moisture is much smaller than at the surface layer,

479 therefore the soil moisture values for S.G. 2 and 3 could be too similar to differentiate. However,
480 for milder slopes (S.G. 1), the higher soil moisture triggering level always applies even down to
481 the deepest soil layer for all the three LSM schemes. ~~In this study, It is also clear to see the~~
482 ~~difference of threshold values amongst different slope groups largely depends on the number of~~
483 ~~landslide events considered, that is with more events considered, the stronger the correlation (e.g.,~~
484 ~~1% exceedance probability means 99% of the events are included for the threshold modelling,~~
485 ~~whilst 50% exceedance probability means half of the data are treated as outliers).~~ The results
486 ~~confirm show~~ that wetter soil ~~indeed~~ can trigger ~~shallow~~ landslides easier in milder slopes than in
487 steeper slopes.

488 All the threshold models are then evaluated under the 45 selected rainfall events (Table 45) using
489 the ROC analysis. ~~Each threshold determined for each of the slope class during the calibration is~~
490 ~~used for the evaluation.~~ The period of the selected rainfall events is between 1 day and 18 days,
491 and the average rainfall intensity ranges from 5.05 mm/day to 24.69 mm/day. ~~For each selected~~
492 ~~event, the number of landslide event is also summarised in the table.~~ The resultant Euclidean
493 distances (d) between each scenario of exceedance probability and the optimal point for ROC
494 analysis are listed in Table 5-6 for all three WRF LSM schemes at the tested exceedance
495 probabilities. The best performance (i.e., lowest d) in each column (i.e., each soil layer of an LSM
496 scheme) is highlighted. In addition, the d results are also plotted in Figure 8 to give a better view
497 of the overall trend amongst different soil layers and LSM schemes. From the figure, for all three
498 LSM schemes at all four soil layers, there is an overall downward and then stabilised trend. Overall
499 for Noah, the simulated surface layer soil moisture provides better landslide monitoring
500 performance than the rest of the soil layers from 1% to 35% exceedance probabilities; and the
501 scheme's worst performance is observed at the third soil layer centred at 70 cm. The values of d

502 for Noah's second and fourth layer are quite close to each other. For Noah-MP, the simulated
503 surface layer soil moisture gives the best performance amongst all four soil layers for most cases
504 between the 1% and 35% exceedance probability range; and the scheme's worst performance is
505 observed at the fourth layer. Unlike Noah, all four soil layers from the Noah-MP scheme provide
506 distinct performance amongst them (i.e., larger d difference). For CLM4, the performance for the
507 surface layer is quite similar to the second layer's, and the differences amongst-between the four
508 layers are small. From the Table 65, it can be seen for Noah the most suitable exceedance
509 probabilities (i.e., the highlighted numbers) range between 35% to 50%; for Noah-MP they are
510 between 30% and 50%;-%, and for CLM4 it stays at 40% for all four soil layers. For both Noah
511 and Noah-MP, the best performance is observed at the surface layer ($d = 0.392$ and $d = 0.369$,
512 respectively), ~~which is in line with their correlation coefficient results against the in-situ~~
513 ~~observations (i.e., the best r value for both LSM schemes is found at the surface layer). (Zhuo,~~
514 ~~2019 #31)~~ Furthermore, the best performance for Noah and Noah-MP follows a regular trend, that
515 is the deeper the soil layer, the poorer the landslide monitoring performance. There are several
516 potential reasons for such an outcome. First, the simulated soil moisture accuracy at the shallower
517 layers are better than the deeper zones. Second, although the wetness conditions at the sliding
518 surface are important, the soil moisture above it is also important (i.e., the loading should be
519 heavier with more water in the upper soil layer). Third, the region has very shallow landslides.
520 Fourth, the WRF modelled soil moisture is not accurate enough in assessing the landslide events
521 in the study region. In order to find out the extract reasons, comprehensive studies with more
522 detailed landslide events datasets are needed in future studies. For CLM4, the best performances
523 show no distinct pattern amongst soil layers (i.e., with the best performance found at the soil Layer
524 3, followed by Layer 2, 1, and 4). Of all the LSM schemes and soil layers, the best performance is

525 found for Noah-MP at the surface layer with 30% exceedance probability ($d=0.369$). Based on the
526 d results, WRF modelled soil moisture provides better landslide prediction performance than the
527 satellite ESA-CCI soil moisture products as shown in our previous study ((Zhuo et al., 2019), i.e.,
528 $d = 0.51$). The ROC curve for the Noah-MP scheme at the surface layer is shown in Figure 9. In
529 the curve, each point represents a scenario with a selected exceedance probability level. It is clear
530 with various exceedance probabilities, FAR can be decreased without sacrificing the HR score (e.g.,
531 4% to 10% exceedance probabilities). At the optimal point at the 30% exceedance probability, the
532 best results for HR and FAR are observed as 0.769 and 0.289, respectively.

533 6. Discussions and Conclusion

534 In this study, the usability of WRF modelled soil moisture for landslide monitoring has been
535 evaluated in the Emilia Romagna region based on the research duration between 2006 and 2015.
536 Specifically, four-layer soil moisture information simulated through the WRF's three most
537 advanced LSM schemes (i.e., Noah, Noah-MP and CLM4) are compared for the purpose. Through
538 the temporal comparison with the in-situ soil moisture observations, it has been found that all three
539 LSM schemes at all four soil layers can produce the general soil moisture's seasonal cycle ~~very~~
540 ~~well~~. However, only Noah-MP is able to simulate the large soil drying phenomenon close to the
541 observations during the drying season, and it also gives the highest correlation coefficient and the
542 lowest $RMSE$ at most soil layers amongst the three LSM schemes. However, it should be noted,
543 the soil moisture evaluation is only based on a single point-based soil moisture sensor that is
544 available in the plain region of the study area. Therefore, the WRF soil moisture performance over
545 the whole study region, in particular, at the mountainous zone cannot be evaluated in this study.
546 Since soil moisture is related to rainfall, we have carried out the WRF rainfall assessments, based
547 on the comparison with the dense rainfall network in the region. The results have shown that there

548 ~~is no distinct difference between the three LSM schemes. The WRF rainfall performance is found~~
549 ~~to be similar to a study carried out over the central USA. For landslide threshold build-up, slope~~
550 ~~information is useful in identifying threshold differences, with threshold becoming smaller for~~
551 ~~steeper area. In other words, dryer soil indeed can trigger landslides in steeper slopes than in milder~~
552 ~~slopes. The result is not surprising, as the slope angle is an importance element of influencing the~~
553 ~~stabilities of earth materials. Further studies~~A landslide prediction model based on soil moisture
554 and -slope angle condition is ~~then carried out~~built up. 17 various exceedance probably levels
555 between 1% and 50% are adopted to find the optimal threshold scenario. Through the ROC
556 analysis of 612 threshold models, the best performance is obtained by the Noah-MP at the surface
557 soil layer with 30% exceedance probability. ~~The outstanding performance of the Noah-MP scheme~~
558 ~~at the surface layer is also in accordance with its high correlation coefficient result found against~~
559 ~~the in-situ observations.~~

560 It should be noted that weighting factors are not considered in the evaluation of the threshold
561 models. Weighting factors can include both social and economic components, for instance, it can
562 include the cost of a disaster event (e.g., both short-term and long-term impacts), the cost of the
563 evacuation (e.g., relocation cost, business shut down), as well as the social impacts of both cases.
564 ~~Nevertheless, i~~In real-life situations, the weighting could play important roles during the final
565 decision making. As for instance, the damages resulted from a missing alarm event could be much
566 more devastating than a false alarm event, or vice versa, and the situation also varies in different
567 regions. Therefore, during operational applications, appropriate weighting factors should be
568 considered.

569 ~~In this study, the~~ WRF is modelled based on the ERA-Interim datasets, however, it has been found
570 in some studies, the performance of using the ERA5 has surpassed the ERA-Interim. Therefore,

571 the ERA5 datasets will be tested in our future studies. Model-based soil moisture estimations could
572 be affected by error accumulation issues, especially in the real-time forecasting mode. A potential
573 solution is to use data assimilation methodologies to correct such errors by assimilating soil
574 moisture information from other data sources. Since in-situ soil moisture sensors are only sparsely
575 available in limited regions, soil moisture measured via satellite remote sensing technologies could
576 provide useful alternatives. Another issue is with the landslide record data, since most of them are
577 based on human experiences (e.g., through newspapers, and victims), a lot of incidences could be
578 unreported. Therefore, the conclusion made here could be biased. One way of expanding the
579 current landslide catalog can depend on automatic landslide detection methods based on remote
580 sensing images.

581 In summary, this study provides an overview of the soil moisture performance of three WRF LSM
582 schemes for landslide hazard assessment. Based on the results, wWe demonstrate that the surface
583 soil moisture (centred at 10 cm) simulated through the Noah-MP LSM scheme is useful in
584 predicting landslide occurrences in the Emilia Romagna region. The highWith the hitting rate of
585 0.769 and the lowfalse alarm rate of 0.289 obtained in this study, show such valuable soil moisture
586 information has the potential-could work in addition to the- in working with rainfall data to provide
587 an efficient landslide early warning system at the regional scalespredictions model. However, one
588 must bear in mind that the results demonstrated in this study are only valid for the selected region.
589 In order to make a general conclusion, more researches are needed using the methodology
590 described in this paper. Particularly, a considerable number of catchments with a broad spectrum
591 of climate and environmental conditions will need to be investigated.

592 **Acknowledgement**

593 This study is supported by Resilient Economy and Society by Integrated SysTems modelling
594 (RESIST), Newton Fund via Natural Environment Research Council (NERC) and Economic and
595 Social Research Council (ESRC) (NE/N012143/1), and the National Natural Science Foundation
596 of China (No: 4151101234). The Landslide inventory data is kindly provided by Dr Matteo Berti,
597 University of Bologna.

598 **References**

599 Berry, P., Garlick, J., and Smith, R.: Near-global validation of the SRTM DEM using satellite
600 radar altimetry, *Remote Sensing of Environment*, 106, 17-27, 2007.

601 Berti, M., Martina, M., Franceschini, S., Pignone, S., Simoni, A., and Pizziolo, M.: Probabilistic
602 rainfall thresholds for landslide occurrence using a Bayesian approach, *Journal of Geophysical*
603 *Research: Earth Surface*, 117, 2012. DOI: <https://doi.org/10.1029/2012JF002367>.

604 Bertolini, G., Guida, M., and Pizziolo, M. J. L.: Landslides in Emilia-Romagna region (Italy):
605 strategies for hazard assessment and risk management, 2, 302-312, 2005.

606 Bittelli, M., Valentino, R., Salvatorelli, F., and Pisa, P. R.: Monitoring soil-water and displacement
607 conditions leading to landslide occurrence in partially saturated clays, *Geomorphology*, 173, 161-
608 173, 2012.

609 Bogaard, T., and Greco, R.: Invited perspectives: Hydrological perspectives on precipitation
610 intensity-duration thresholds for landslide initiation: proposing hydro-meteorological thresholds,
611 *Natural Hazards and Earth System Sciences*, 18, 31-39, 2018.

612 Cai, X., Yang, Z. L., Xia, Y., Huang, M., Wei, H., Leung, L. R., and Ek, M. B.: Assessment of
613 simulated water balance from Noah, Noah-MP, CLM, and VIC over CONUS using the NLDAS
614 test bed, *Journal of Geophysical Research: Atmospheres*, 119, 13,751-713,770, 2014.

615 Cai, X.: Hydrological assessment and biogeochemical advancement of the Noah-MP land surface
616 model, Doctor of Philosophy, Geological Sciences, The University of Texas at Austin, 164 pp.,
617 2015.

618 Chae, B.-G., Park, H.-J., Catani, F., Simoni, A., and Berti, M.: Landslide prediction, monitoring
619 and early warning: a concise review of state-of-the-art, *Geosciences Journal*, 21, 1033-1070, 2017.

620 Chen, F., and Dudhia, J.: Coupling an advanced land surface-hydrology model with the Penn State-
621 NCAR MM5 modeling system. Part I: Model implementation and sensitivity, *Monthly Weather*
622 *Review*, 129, 569-585, 2001.

623 Ciabatta, L., Camici, S., Brocca, L., Ponziani, F., Stelluti, M., Berni, N., and Moramarco, T. J. J.
624 o. H.: Assessing the impact of climate-change scenarios on landslide occurrence in Umbria Region,
625 *Italy*, 541, 285-295, 2016.

626 Crozier, M. J.: Prediction of rainfall-triggered landslides: A test of the antecedent water status
627 model, *Earth surface processes and landforms*, 24, 825-833, 1999.

628 Dee, D. P., Uppala, S. M., Simmons, A., Berrisford, P., Poli, P., Kobayashi, S., Andrae, U.,
629 Balmaseda, M., Balsamo, G., and Bauer, d. P.: The ERA-Interim reanalysis: Configuration and
630 performance of the data assimilation system, *Quarterly Journal of the royal meteorological society*,
631 137, 553-597, 2011.

632 Dorigo, W., Wagner, W., Albergel, C., Albrecht, F., Balsamo, G., Brocca, L., Chung, D., Ertl, M.,
633 Forkel, M., and Gruber, A.: ESA CCI Soil Moisture for improved Earth system understanding:
634 State-of-the art and future directions, *Remote Sensing of Environment*, 203, 185-215, 2017.

635 Dudhia, J.: Numerical study of convection observed during the winter monsoon experiment using
636 a mesoscale two-dimensional model, *Journal of the Atmospheric Sciences*, 46, 3077-3107, 1989.

637 Ek, M., Mitchell, K., Lin, Y., Rogers, E., Grunmann, P., Koren, V., Gayno, G., and Tarpley, J.:
638 Implementation of Noah land surface model advances in the National Centers for Environmental
639 Prediction operational mesoscale Eta model, *Journal of Geophysical Research: Atmospheres*, 108,
640 2003. DOI: <https://doi.org/10.1029/2002JD003296>.

641 Fawcett, T.: An introduction to ROC analysis, *Pattern recognition letters*, 27, 861-874, 2006.

642 Gariano, S. L., Brunetti, M. T., Iovine, G., Melillo, M., Peruccacci, S., Terranova, O., Vennari, C.,
643 and Guzzetti, F.: Calibration and validation of rainfall thresholds for shallow landslide forecasting
644 in Sicily, southern Italy, *Geomorphology*, 228, 653-665, 2015.

645 Gilliland, E. K., and Rowe, C. M.: A comparison of cumulus parameterization schemes in the
646 WRF model, Proceedings of the 87th AMS Annual Meeting & 21th Conference on Hydrology,
647 2007,

648 Glade, T., Crozier, M., and Smith, P.: Applying probability determination to refine landslide-
649 triggering rainfall thresholds using an empirical “Antecedent Daily Rainfall Model”, Pure and
650 Applied Geophysics, 157, 1059-1079, 2000.

651 Greve, P., Warrach-Sagi, K., and Wulfmeyer, V.: Evaluating soil water content in a WRF-Noah
652 downscaling experiment, Journal of Applied Meteorology and Climatology, 52, 2312-2327, 2013.

653 Hawke, R., and McConchie, J.: In situ measurement of soil moisture and pore-water pressures in
654 an ‘incipient’ landslide: Lake Tutira, New Zealand, Journal of environmental management, 92,
655 266-274, 2011.

656 Hong, S.-Y., Noh, Y., and Dudhia, J.: A new vertical diffusion package with an explicit treatment
657 of entrainment processes, Monthly Weather Review, 134, 2318-2341, 2006.

658 Hosmer, D., and Lemeshow, S.: Applied logistic regression. 1989, New York: Johns Wiley & Sons,
659 1989.

660 Jiménez, P. A., Dudhia, J., González-Rouco, J. F., Navarro, J., Montávez, J. P., and García-
661 Bustamante, E.: A revised scheme for the WRF surface layer formulation, Monthly Weather
662 Review, 140, 898-918, 2012.

663 Jordan, R.: A one-dimensional temperature model for a snow cover: Technical documentation for
664 SNTHERM. 89, Cold Regions Research and Engineering Laboratory, 1991.

665 Kain, J. S.: The Kain-Fritsch convective parameterization: An update, Journal of Applied
666 Meteorology, 43, 2004. DOI: [http://dx.doi.org/10.1175/1520-
667 0450\(2004\)043<0170:TKCPAU>2.0.CO;2](http://dx.doi.org/10.1175/1520-0450(2004)043<0170:TKCPAU>2.0.CO;2).

668 Klose, M., Highland, L., Damm, B., and Terhorst, B.: Estimation of Direct Landslide Costs in
669 Industrialized Countries: Challenges, Concepts, and Case Study, in: Landslide Science for a Safer
670 Geoenvironment, World Landslide Forum 3, China (Beijing), 2014, 661-667,

671 Lagomarsino, D., Segoni, S., Fanti, R., and Catani, F. J. L.: Updating and tuning a regional-scale
672 landslide early warning system, 10, 91-97, 2013.

673 Lagomarsino, D., Segoni, S., Rosi, A., Rossi, G., Battistini, A., Catani, F., Casagli, N. J. N. H.,
674 and Sciences, E. S.: Quantitative comparison between two different methodologies to define
675 rainfall thresholds for landslide forecasting, 15, 2413-2423, 2015.

676 Lawrence, D. M., and Slater, A. G.: Incorporating organic soil into a global climate model, *Climate*
677 *Dynamics*, 30, 145-160, 2008.

678 Lawrence, D. M., Oleson, K. W., Flanner, M. G., Thornton, P. E., Swenson, S. C., Lawrence, P.
679 J., Zeng, X., Yang, Z. L., Levis, S., and Sakaguchi, K.: Parameterization improvements and
680 functional and structural advances in version 4 of the Community Land Model, *Journal of*
681 *Advances in Modeling Earth Systems*, 3, 27, 2011.

682 Lawrence, D. M., Oleson, K. W., Flanner, M. G., Fletcher, C. G., Lawrence, P. J., Levis, S.,
683 Swenson, S. C., and Bonan, G. B.: The CCSM4 land simulation, 1850–2005: Assessment of
684 surface climate and new capabilities, *Journal of Climate*, 25, 2240-2260, 2012.

685 Leung, L. R., and Qian, Y.: Atmospheric rivers induced heavy precipitation and flooding in the
686 western US simulated by the WRF regional climate model, *Geophysical research letters*, 36, 2009.
687 DOI: <https://doi.org/10.1029/2008GL036445>.

688 Liang, X., Xie, Z., and Huang, M.: A new parameterization for surface and groundwater
689 interactions and its impact on water budgets with the variable infiltration capacity (VIC) land
690 surface model, *Journal of Geophysical Research: Atmospheres*, 108, 2003. DOI:
691 <https://doi.org/10.1029/2002JD003090>.

692 Maheu, A., Anctil, F., Gaborit, É., Fortin, V., Nadeau, D. F., and Therrien, R.: A field evaluation
693 of soil moisture modelling with the Soil, Vegetation, and Snow (SVS) land surface model using
694 evapotranspiration observations as forcing data, *Journal of Hydrology*, 558, 532-545, 2018.

695 Martelloni, G., Segoni, S., Fanti, R., and Catani, F. J. L.: Rainfall thresholds for the forecasting of
696 landslide occurrence at regional scale, 9, 485-495, 2012.

697 Mlawer, E. J., Taubman, S. J., Brown, P. D., Iacono, M. J., and Clough, S. A.: Radiative transfer
698 for inhomogeneous atmospheres: RRTM, a validated correlated-k model for the longwave, *Journal*
699 *of Geophysical Research: Atmospheres*, 102, 16663-16682, 1997.

700 Niu, G. Y., Yang, Z. L., Dickinson, R. E., and Gulden, L. E.: A simple TOPMODEL-based runoff
701 parameterization (SIMTOP) for use in global climate models, *Journal of Geophysical Research:*
702 *Atmospheres*, 110, 2005. DOI: <https://doi.org/10.1029/2005JD006111>.

703 Niu, G. Y., Yang, Z. L., Dickinson, R. E., Gulden, L. E., and Su, H.: Development of a simple
704 groundwater model for use in climate models and evaluation with Gravity Recovery and Climate
705 Experiment data, *Journal of Geophysical Research: Atmospheres*, 112, 2007. DOI:
706 <https://doi.org/10.1029/2006JD007522>.

707 Niu, G. Y., Yang, Z. L., Mitchell, K. E., Chen, F., Ek, M. B., Barlage, M., Kumar, A., Manning,
708 K., Niyogi, D., and Rosero, E.: The community Noah land surface model with
709 multiparameterization options (Noah-MP): 1. Model description and evaluation with local-scale
710 measurements, *Journal of Geophysical Research: Atmospheres*, 116, 2011. DOI:
711 <https://doi.org/10.1029/2010JD015139>.

712 Oleson, K., Niu, G. Y., Yang, Z. L., Lawrence, D., Thornton, P., Lawrence, P., Stöckli, R.,
713 Dickinson, R., Bonan, G., and Levis, S.: Improvements to the Community Land Model and their
714 impact on the hydrological cycle, *Journal of Geophysical Research: Biogeosciences (2005–2012)*,
715 113, 2008.

716 Oleson, K. W., Lawrence, D. M., Gordon, B., Flanner, M. G., Kluzek, E., Peter, J., Levis, S.,
717 Swenson, S. C., Thornton, E., and Feddema, J.: Technical description of version 4.0 of the
718 Community Land Model (CLM), 2010.

719 Pistocchi, A., Bouraoui, F., and Bittelli, M.: A simplified parameterization of the monthly topsoil
720 water budget, *Water Resources Research*, 44, 2008. DOI: <https://doi.org/10.1029/2007WR006603>.

721 Ponziani, F., Pandolfo, C., Stelluti, M., Berni, N., Brocca, L., and Moramarco, T. J. L.: Assessment
722 of rainfall thresholds and soil moisture modeling for operational hydrogeological risk prevention
723 in the Umbria region (central Italy), 9, 229-237, 2012.

724 Posner, A. J., and Georgakakos, K. P.: Soil moisture and precipitation thresholds for real-time
725 landslide prediction in El Salvador, *Landslides*, 12, 1179-1196, 2015.

726 Rossi, M., Witt, A., Guzzetti, F., Malamud, B. D., Peruccacci, S. J. E. S. P., and Landforms:
727 Analysis of historical landslide time series in the Emilia-Romagna region, northern Italy, 35, 1123-
728 1137, 2010.

729 Segoni, S., Lagomarsino, D., Fanti, R., Moretti, S., and Casagli, N.: Integration of rainfall
730 thresholds and susceptibility maps in the Emilia Romagna (Italy) regional-scale landslide warning
731 system, *Landslides*, 12, 773-785, 2015.

732 Segoni, S., Rosi, A., Fanti, R., Gallucci, A., Monni, A., and Casagli, N. J. W.: A Regional-Scale
733 Landslide Warning System Based on 20 Years of Operational Experience, 10, 1297, 2018a.

734 Segoni, S., Rosi, A., Lagomarsino, D., Fanti, R., and Casagli, N.: Brief communication: Using
735 averaged soil moisture estimates to improve the performances of a regional-scale landslide early
736 warning system, *Natural Hazards and Earth System Sciences*, 18, 807-812, 2018b.

737 Skamarock, W., Klemp, J., Dudhia, J., Gill, D., Barker, D., Duda, M., Huang, X., Wang, W., and
738 Powers, J.: A description of the advanced research WRF Version 3, NCAR technical note,
739 Mesoscale and Microscale Meteorology Division, National Center for Atmospheric Research,
740 Boulder, Colorado, USA, 2008.

741 Skamarock, W. C., Klemp, J. B., Dudhia, J., Gill, D. O., Barker, D. M., Wang, W., and Powers, J.
742 G.: A description of the advanced research WRF version 2, National Center For Atmospheric
743 Research Boulder Co Mesoscale and Microscale Meteorology Div, 2005.

744 Srivastava, P. K., Han, D., Rico-Ramirez, M. A., Al-Shrafany, D., and Islam, T.: Data fusion
745 techniques for improving soil moisture deficit using SMOS satellite and WRF-NOAH land surface
746 model, *Water resources management*, 27, 5069-5087, 2013a.

747 Srivastava, P. K., Han, D., Rico Ramirez, M. A., and Islam, T.: Comparative assessment of
748 evapotranspiration derived from NCEP and ECMWF global datasets through Weather Research
749 and Forecasting model, *Atmospheric Science Letters*, 14, 118-125, 2013b.

750 Srivastava, P. K., Han, D., Rico-Ramirez, M. A., O'Neill, P., Islam, T., Gupta, M., and Dai, Q.:
751 Performance evaluation of WRF-Noah Land surface model estimated soil moisture for

752 hydrological application: Synergistic evaluation using SMOS retrieved soil moisture, *Journal of*
753 *Hydrology*, 529, 200-212, 2015.

754 Stéfanon, M., Drobinski, P., D'Andrea, F., Lebeau-pin-Brossier, C., and Bastin, S.: Soil moisture-
755 temperature feedbacks at meso-scale during summer heat waves over Western Europe, *Climate*
756 *dynamics*, 42, 1309-1324, 2014.

757 Temimi, M., Leconte, R., Chaouch, N., Sukumal, P., Khanbilvardi, R., and Brissette, F.: A
758 combination of remote sensing data and topographic attributes for the spatial and temporal
759 monitoring of soil wetness, *Journal of Hydrology*, 388, 28-40, 2010.

760 Thompson, G., Field, P. R., Rasmussen, R. M., and Hall, W. D.: Explicit forecasts of winter
761 precipitation using an improved bulk microphysics scheme. Part II: Implementation of a new snow
762 parameterization, *Monthly Weather Review*, 136, 5095-5115, 2008.

763 Tsai, T.-L., and Chen, H.-F.: Effects of degree of saturation on shallow landslides triggered by
764 rainfall, *Environmental Earth Sciences*, 59, 1285-1295, 2010.

765 Valenzuela, P., Domínguez-Cuesta, M. J., García, M. A. M., and Jiménez-Sánchez, M.: Rainfall
766 thresholds for the triggering of landslides considering previous soil moisture conditions (Asturias,
767 NW Spain), *Landslides*, 15, 273-282, 2018.

768 Van Den Broeke, M. S., Kalin, A., Alavez, J. A. T., Oglesby, R., Hu, Q. J. T., and climatology, a.:
769 A warm-season comparison of WRF coupled to the CLM4. 0, Noah-MP, and Bucket hydrology
770 land surface schemes over the central USA, 134, 801-816, 2018.

771 Wei, J., Dirmeyer, P. A., Guo, Z., Zhang, L., and Misra, V.: How much do different land models
772 matter for climate simulation? Part I: Climatology and variability, *Journal of Climate*, 23, 3120-
773 3134, 2010.

774 Wharton, S., Simpson, M., Osuna, J., Newman, J., and Biraud, S.: Assessment of Land Surface
775 Model Performance in WRF for Simulating Wind at Heights Relevant to the Wind Energy
776 Community, Lawrence Livermore National Lab.(LLNL), Livermore, CA (United States), 2013.

777 Wilks, D.: *Statistical Methods in the Atmospheric Sciences*, 3rd ed., Academic Press, 2011.

778 Yang, Z. L., Niu, G. Y., Mitchell, K. E., Chen, F., Ek, M. B., Barlage, M., Longuevergne, L.,
779 Manning, K., Niyogi, D., and Tewari, M.: The community Noah land surface model with
780 multiparameterization options (Noah-MP): 2. Evaluation over global river basins, *Journal of*
781 *Geophysical Research: Atmospheres*, 116, 2011.

782 Zaidi, S. M., and Gisen, J. I. A.: Evaluation of Weather Research and Forecasting (WRF)
783 Microphysics single moment class-3 and class-6 in Precipitation Forecast, *MATEC Web of*
784 *Conferences*, 2018, 03007,

785 Zaitchik, B. F., Santanello, J. A., Kumar, S. V., and Peters-Lidard, C. D.: Representation of soil
786 moisture feedbacks during drought in NASA unified WRF (NU-WRF), *Journal of*
787 *Hydrometeorology*, 14, 360-367, 2013.

788 Zeng, X., and Decker, M.: Improving the numerical solution of soil moisture-based Richards
789 equation for land models with a deep or shallow water table, *Journal of Hydrometeorology*, 10,
790 308-319, 2009.

791 Zhao, B., Dai, Q., Han, D., Dai, H., Mao, J., and Zhuo, L.: Antecedent wetness and rainfall
792 information in landslide threshold definition, *Hydrol. Earth Syst. Sci. Discuss.*, 2019, 1-26,
793 10.5194/hess-2019-150, 2019a.

794 Zhao, B., Dai, Q., Han, D., Dai, H., Mao, J., and Zhuo, L. J. J. o. H.: Probabilistic thresholds for
795 landslides warning by integrating soil moisture conditions with rainfall thresholds, *574*, 276-287,
796 2019b.

797 Zhuo, L., Dai, Q., and Han, D.: Evaluation of SMOS soil moisture retrievals over the central United
798 States for hydro-meteorological application, *Physics and Chemistry of the Earth, Parts A/B/C*, 83,
799 146-155, 2015a.

800 Zhuo, L., Han, D., Dai, Q., Islam, T., and Srivastava, P. K.: Appraisal of NLDAS-2 multi-model
801 simulated soil moistures for hydrological modelling, *Water resources management*, 29, 3503-3517,
802 2015b.

803 Zhuo, L., Dai, Q., Han, D., Chen, N., Zhao, B., and Berti, M.: Evaluation of remotely sensed soil
804 moisture for landslide hazard assessment, *IEEE Journal of Selected Topics in Applied Earth*
805 *Observations and Remote Sensing*, 12, 162 - 173, 2019.

806
807

Table 1. Comparison of Noah, Noah-MP, and CLM4.

	Noah	Noah-MP	CLM4
Energy balance	Yes	Yes	Yes
Water balance	Yes	Yes	Yes
No. of soil layers	4	4	10
Depth of total soil column	2.0 m	2.0 m	3.802 m
Model soil layer thickness	0.1, 0.3, 0.6, 1.0 m	0.1, 0.3, 0.6, 1.0 m	0.018, 0.028, 0.045, 0.075, 0.124, 0.204, 0.336, 0.553, 0.913, 1.506 m
No. of vegetation layers	A single combined surface layer of vegetation and snow	Single layer	Single layer
Vegetation	Dominant vegetation type in one grid cell with prescribed LAI	Dominant vegetation type in one grid cell with dynamic LAI	Up to 10 vegetation types in one grid cell with prescribed LAI
No. of snow layers	A single combined surface layer of vegetation and snow	Up to three layers	Up to five layers

Table 2. WRF parameterizations used in this study.

	Settings/ Parameterizations	References
Map projection	Lambert	
Central point of domain	Latitude: 44.54; Longitude: 11.02	
Latitudinal grid length	5 km	
Longitudinal grid length	5 km	
Model output time step	Daily	
Nesting	Two-way	
Land surface model	Noah, Noah-MP, CLM	
Simulation period	1/1/2006 – 31/12/2015	
Spin-up period	1/1/2005 – 31/12/2005	
Microphysics	New Thompson	(Thompson et al., 2008)
Shortwave radiation	Dudhia scheme	(Dudhia, 1989)
Longwave radiation	Rapid Radiative Transfer Model	(Mlawer et al., 1997)
Surface layer	Revised MM5	(Jiménez et al., 2012; Chen and Dudhia, 2001)
Planetary boundary layer	Yonsei University method	(Hong et al., 2006)
Cumulus Parameterization	Kain-Fritsch (new Eta) scheme	(Kain, 2004)

Table 3. Statistical summary of the WRF performance in simulating soil moisture for different soil layers, based on comparison with the [single point](#) in-situ observations.

	<i>R</i>				<i>RMSE (m³/m³)</i>			
	0.10 m	0.25 m	0.70 m	1.50 m	0.1 m	0.25 m	0.70 m	1.50 m
Noah	0.728	0.645	0.660	0.430	0.123	0.125	0.141	0.055
Noah-MP	0.809	0.683	0.738	0.498	0.060	0.070	0.088	0.092
CLM	0.789	0.743	0.648	0.287	0.089	0.087	0.123	0.089

Table 4. Statistical summary of the WRF performance in simulating rainfall for the whole study region, based on comparison with the in-situ rainfall network.

	<i>R</i>			<i>RMSE (mm)</i>		
	Noah	Noah-MP	CLM4	Noah	Noah-MP	CLM4
Min	0.094	0.090	0.076	4.275	4.286	4.219
Max	0.779	0.798	0.801	19.814	19.178	19.476
Mean	0.425	0.426	0.421	7.772	7.719	7.943
0.25 percentile	0.147	0.130	0.154	4.579	4.297	4.438
0.50 percentile	0.189	0.153	0.210	4.951	4.909	4.910
0.75 percentile	0.192	0.183	0.211	5.006	4.970	5.010

Table 5. Rainfall events information.

Starting date			Ending date			Duration (days)	Rainfall intensity (mm/day)	Number of Landslide events
Year	Month	Day	Year	Month	Day			
2014	1	13	2014	1	24	12	20.50	2
2014	1	28	2014	2	14	18	13.61	0
2014	2	26	2014	3	6	9	13.35	0
2014	3	22	2014	3	27	6	11.08	0
2014	4	4	2014	4	5	2	18.98	0
2014	4	27	2014	5	4	8	12.13	0
2014	5	26	2014	6	3	9	5.05	0
2014	6	14	2014	6	16	3	18.29	0
2014	6	25	2014	6	30	6	11.39	0
2014	7	7	2014	7	14	8	7.84	0
2014	7	21	2014	7	30	10	15.35	0
2014	8	31	2014	9	5	6	5.67	0
2014	9	10	2014	9	12	3	11.84	0
2014	9	19	2014	9	20	2	23.04	0
2014	10	1	2014	10	1	1	14.51	0
2014	10	10	2014	10	17	8	13.01	0
2014	11	4	2014	11	18	15	18.28	0
2014	11	25	2014	12	7	13	7.58	0
2014	12	13	2014	12	16	4	6.24	0
2015	1	16	2015	1	17	2	14.87	0
2015	1	21	2015	1	23	3	7.13	0
2015	1	29	2015	2	10	13	9.98	0
2015	2	13	2015	2	17	5	6.62	1
2015	2	21	2015	2	26	6	11.84	4
2015	3	3	2015	3	7	5	11.69	1
2015	3	15	2015	3	17	3	9.00	0
2015	3	21	2015	3	27	7	12.09	2
2015	4	3	2015	4	5	3	16.62	0
2015	4	17	2015	4	18	2	6.99	0
2015	4	26	2015	4	29	4	11.23	0
2015	5	15	2015	5	16	2	8.83	0
2015	5	20	2015	5	27	8	10.58	1
2015	6	8	2015	6	11	4	6.47	0
2015	6	16	2015	6	19	4	13.44	0
2015	6	23	2015	6	24	2	6.07	0
2015	7	22	2015	7	25	4	6.05	0
2015	8	9	2015	8	10	2	24.69	0
2015	8	15	2015	8	19	5	10.69	0
2015	8	23	2015	8	24	2	7.88	0
2015	9	13	2015	9	14	2	24.66	1
2015	9	23	2015	9	24	2	7.50	0
2015	10	1	2015	10	7	7	13.73	0
2015	10	10	2015	10	19	10	9.40	0
2015	10	27	2015	10	29	3	20.33	0
2015	11	21	2015	11	25	5	13.78	1

Table 6. Results of Euclidean distances (d) between individual points and the optimal point for ROC analysis are listed. The best performance (i.e., lowest d) for each column (i.e., each soil layer of an LSM scheme) is highlighted. The optimal performance of all is highlighted in red.

<i>e.p.</i> (%)	Noah				Noah-MP				CLM4			
	10 cm	25 cm	70 cm	150 cm	10 cm	25 cm	70 cm	150 cm	10 cm	25 cm	70 cm	150 cm
1	0.942	0.971	0.962	0.947	0.857	0.937	0.897	0.963	0.942	0.939	0.978	0.975
2	0.906	0.945	0.963	0.923	0.854	0.912	0.883	0.959	0.923	0.922	0.959	0.952
3	0.889	0.924	0.961	0.915	0.849	0.855	0.838	0.952	0.870	0.874	0.940	0.947
4	0.884	0.898	0.946	0.914	0.838	0.814	0.829	0.924	0.831	0.843	0.925	0.947
5	0.860	0.875	0.924	0.896	0.820	0.793	0.812	0.908	0.791	0.822	0.915	0.921
6	0.835	0.854	0.910	0.874	0.803	0.785	0.800	0.905	0.770	0.817	0.911	0.909
7	0.827	0.861	0.902	0.858	0.777	0.767	0.791	0.889	0.753	0.801	0.902	0.900
8	0.816	0.849	0.889	0.851	0.745	0.765	0.782	0.876	0.745	0.785	0.902	0.910
9	0.790	0.827	0.878	0.834	0.706	0.732	0.766	0.871	0.742	0.777	0.864	0.904
10	0.762	0.811	0.863	0.825	0.672	0.702	0.747	0.862	0.738	0.767	0.835	0.887
15	0.615	0.741	0.839	0.763	0.560	0.629	0.716	0.835	0.702	0.700	0.729	0.790
20	0.485	0.627	0.779	0.652	0.515	0.571	0.624	0.774	0.570	0.602	0.594	0.650
25	0.432	0.544	0.728	0.512	0.403	0.465	0.574	0.736	0.509	0.522	0.471	0.509
30	0.437	0.495	0.643	0.451	0.369	0.375	0.544	0.679	0.475	0.477	0.447	0.469
35	0.392	0.446	0.592	0.436	0.390	0.404	0.411	0.498	0.441	0.435	0.428	0.430
40	0.500	0.407	0.531	0.416	0.439	0.385	0.382	0.436	0.406	0.405	0.398	0.410
50	0.552	0.425	0.404	0.411	0.489	0.417	0.416	0.429	0.437	0.435	0.408	0.437

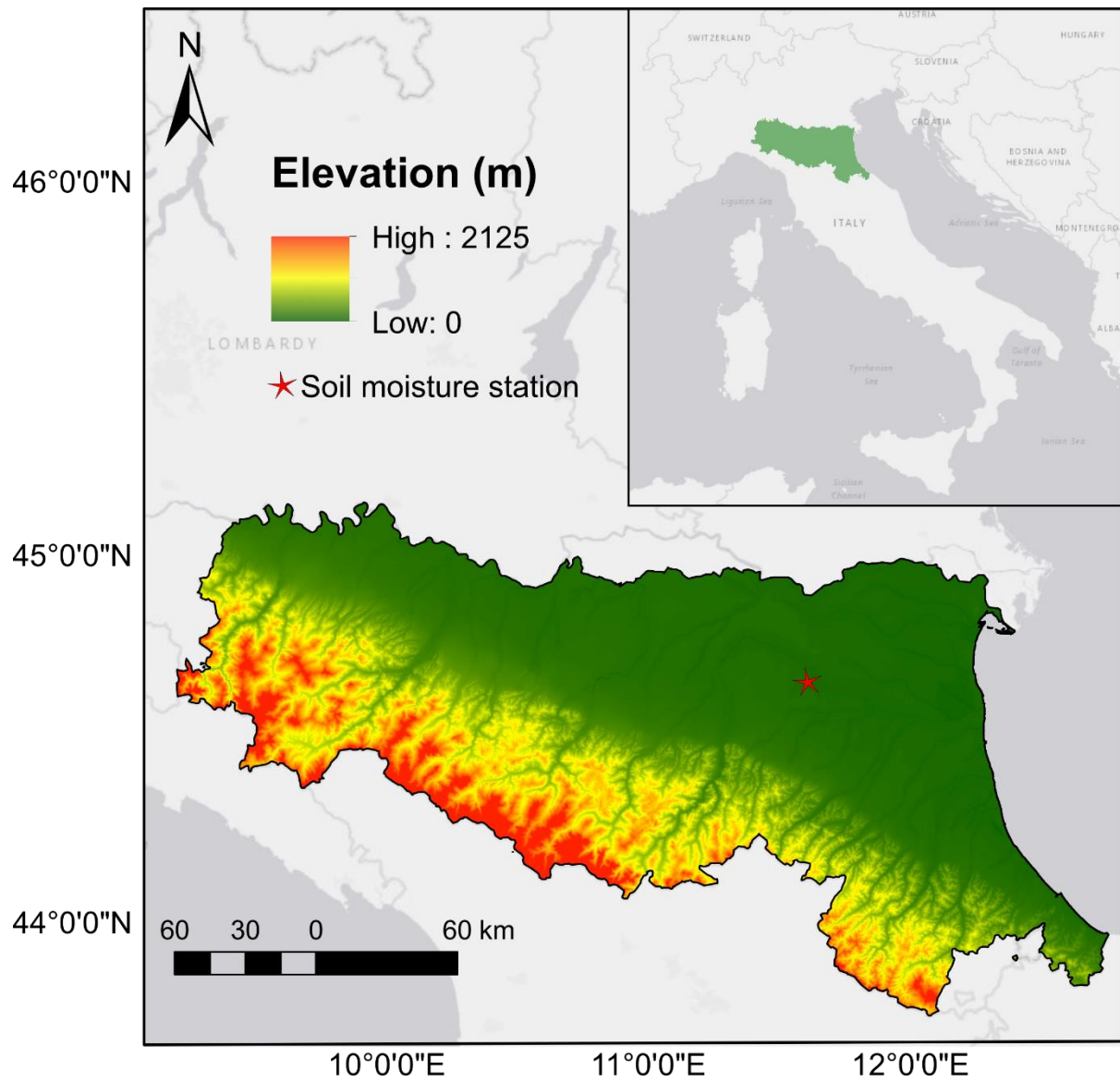


Figure 1. Location of the Emilia Romagna Region with elevation map and in-situ soil moisture station also shown.

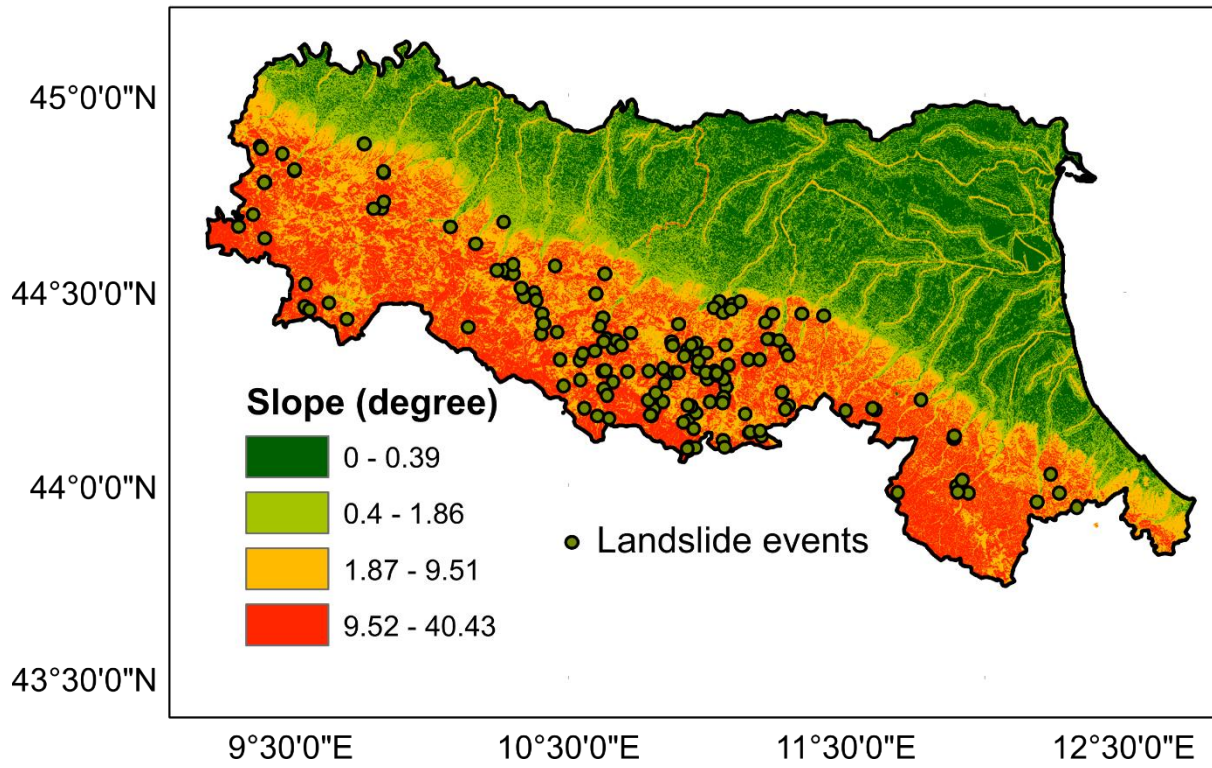


Figure 2. Landslide events with slope angle map.

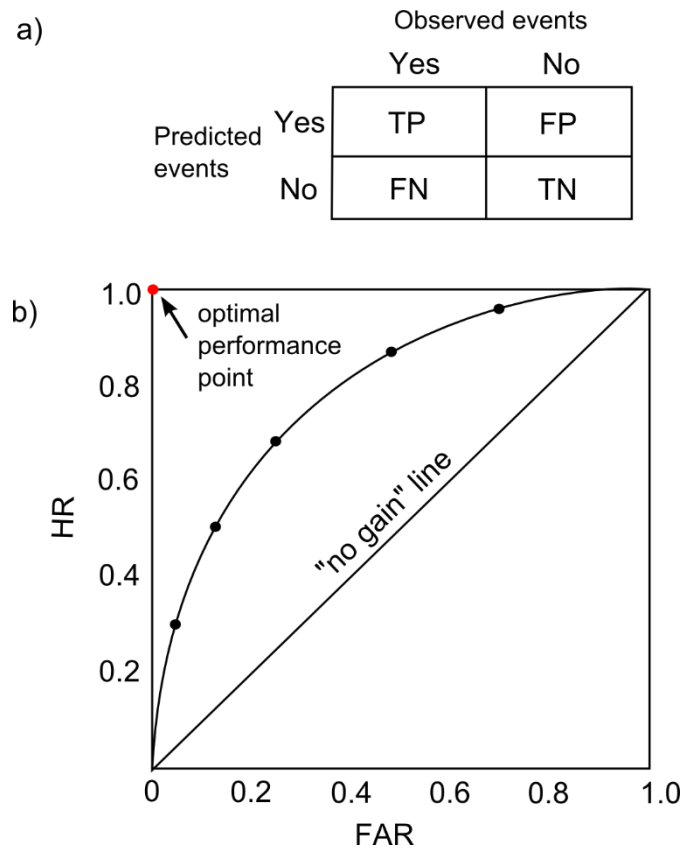


Figure 3. a) Contingency table illustrates the four possible outcomes of a binary classifier model: TP (True Positive), TN (True Negative), FP (False Positive), and FN (False Negative). b) ROC (Receiver Operating Characteristic) analysis with HR (Hitting Rate) against FAR (False Alarm Rate).

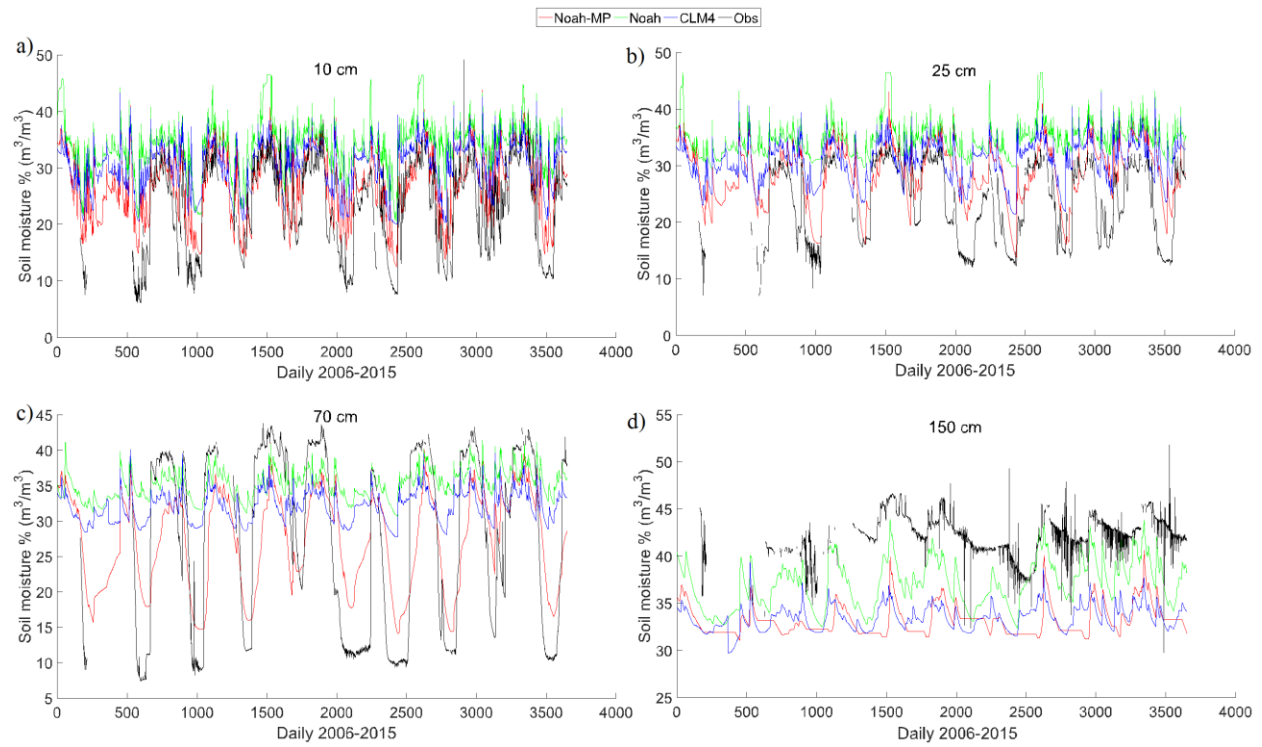


Figure 4. Soil moisture temporal variations of WRF simulations and in-situ observations for four soil layers at a) 10 cm; b) 25 cm; c) 70 cm; and d) 150 cm.

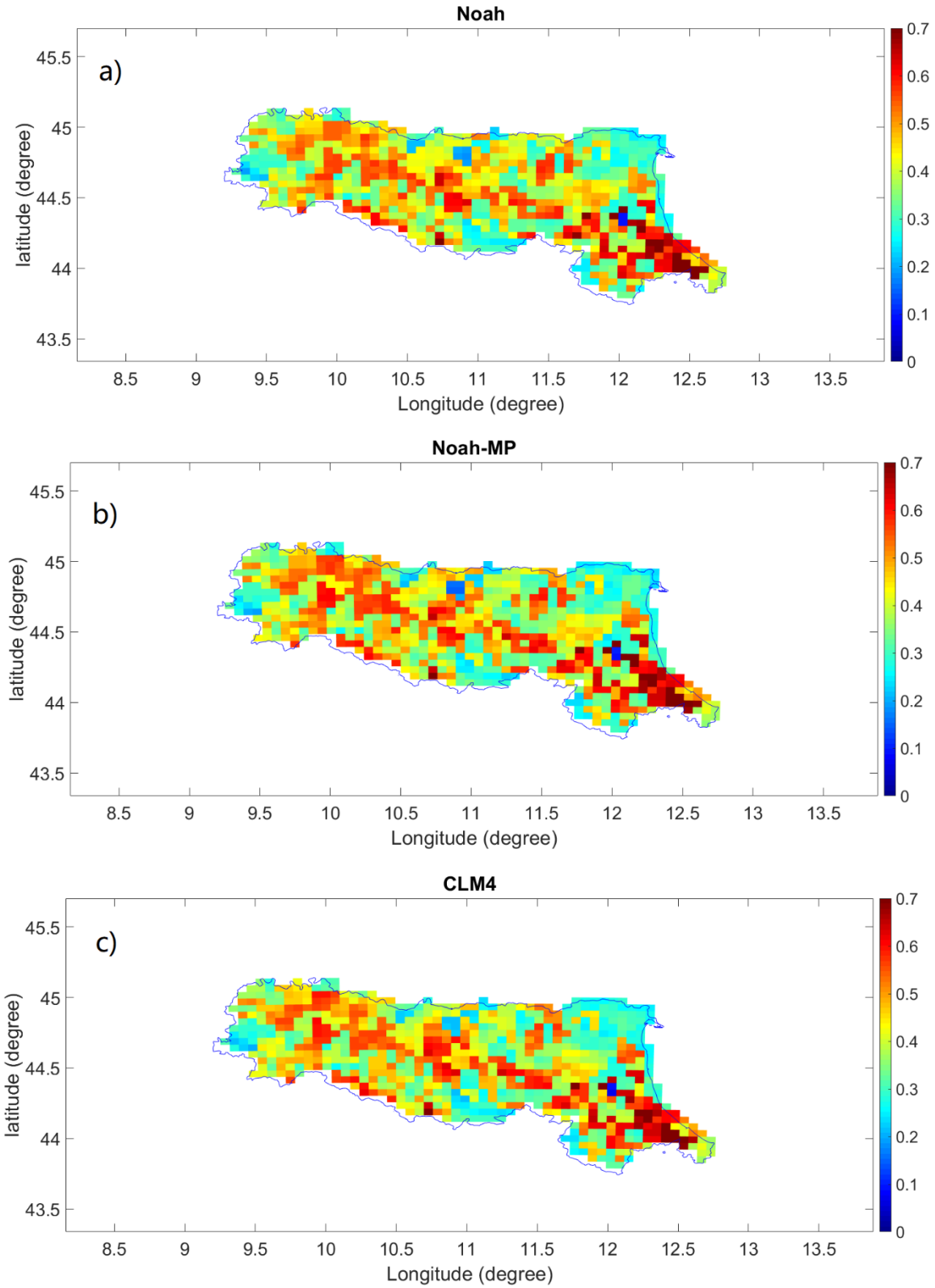


Figure 5. Rainfall evaluation: spatial distribution of the correlation coefficient R of a) Noah, b) Noah-MP and c) CLM4.

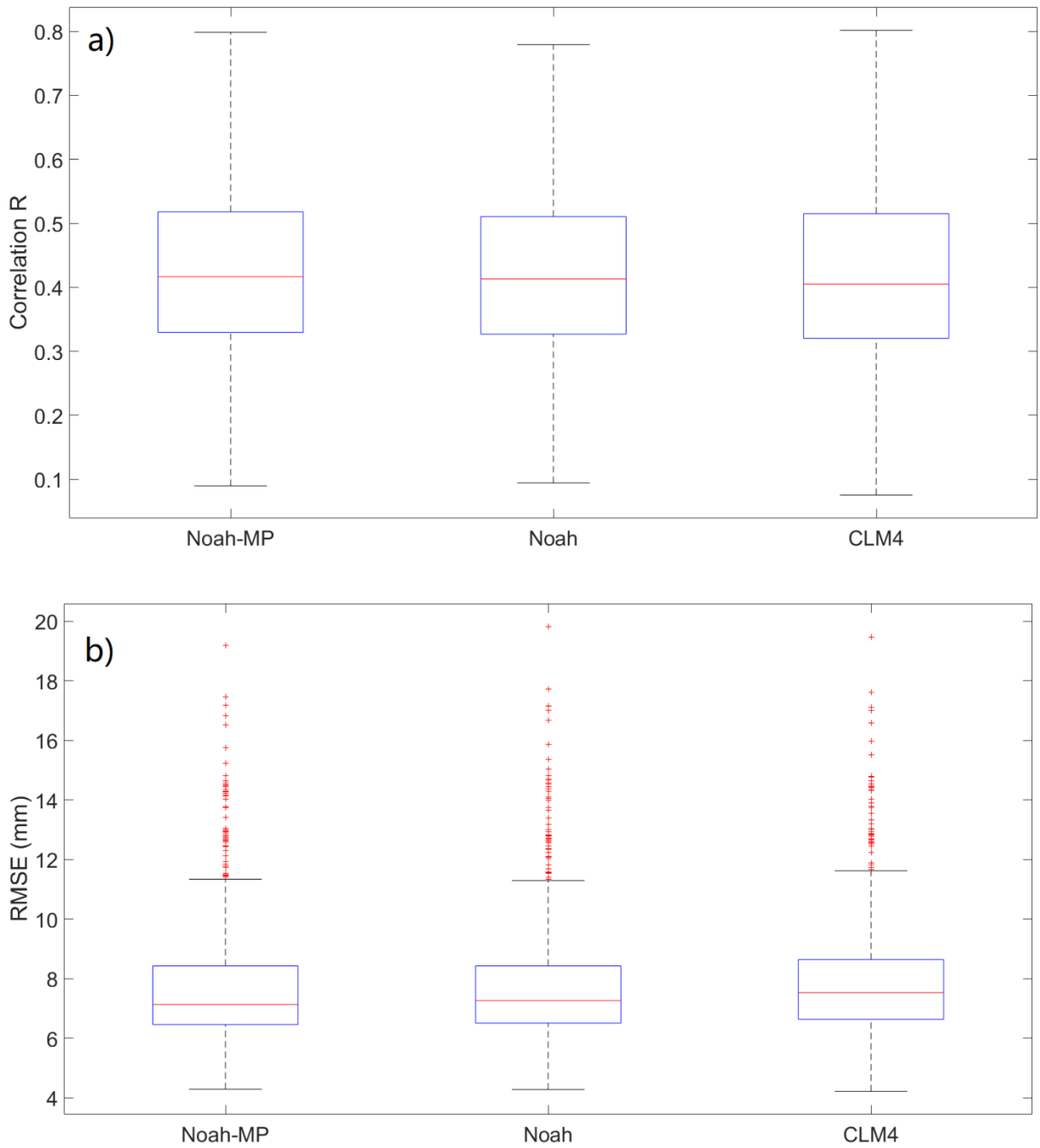


Figure 6. Boxplots of rainfall evaluation results of a) R and b) $RMSE$: minimum, maximum, 0.25, 0.50 and 0.75 percentiles, and outliers (red cross).

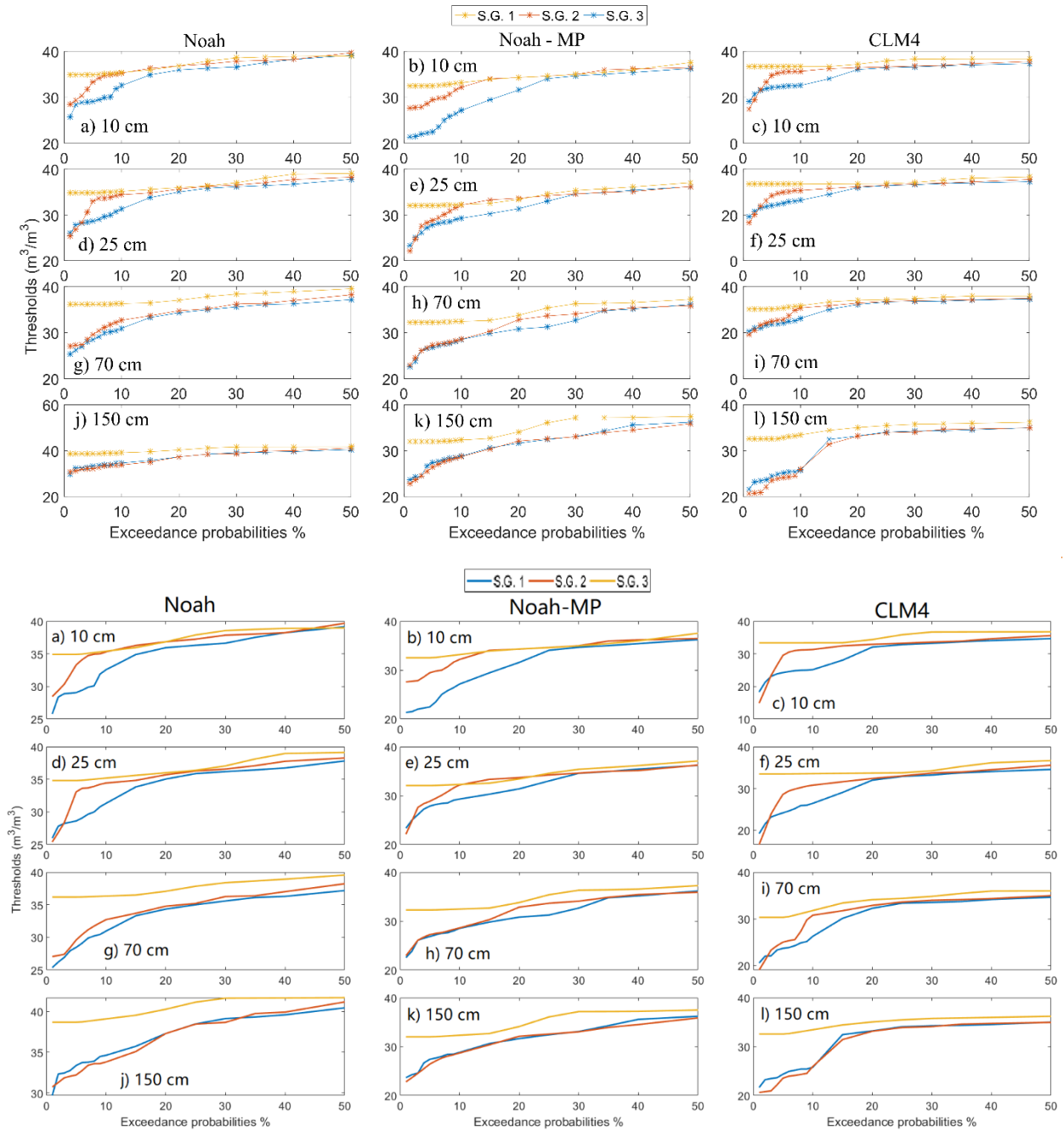


Figure 7. Threshold plots. For Noah (a, d, g, j), Noah-MP (b, e, h, k), and CLM4 (c, f, i, l) land surface schemes under three Slope angle Groups (S.G.) with S.G. 1 = 0.4-1.86°; S.G. 2 = 1.87-9.61°; S.G. 3 = 9.52-40.43°.

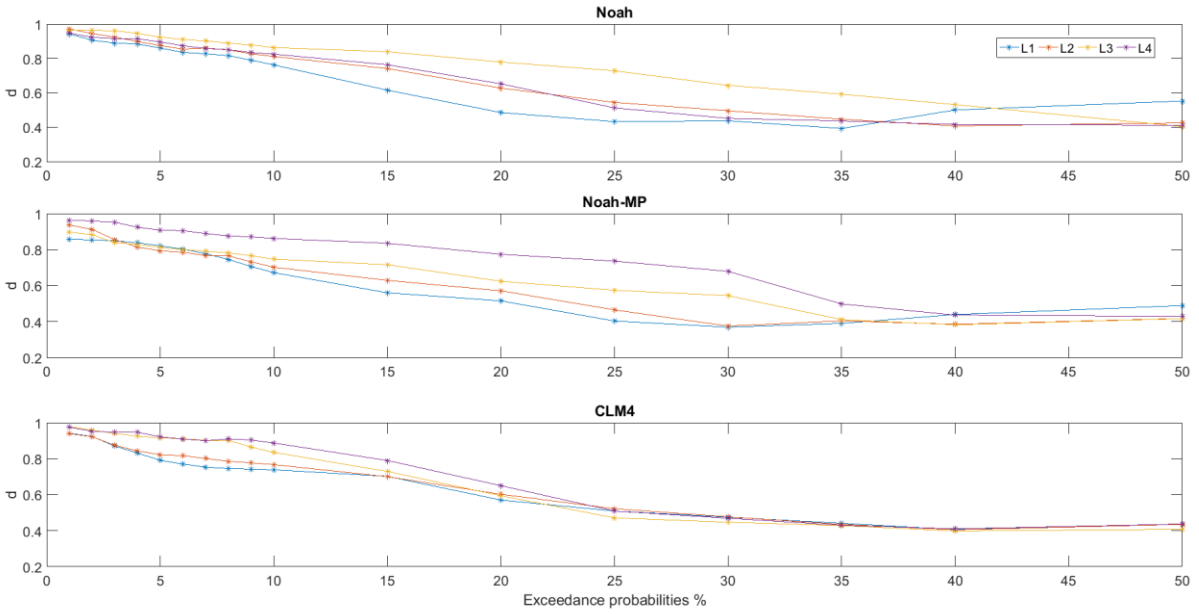
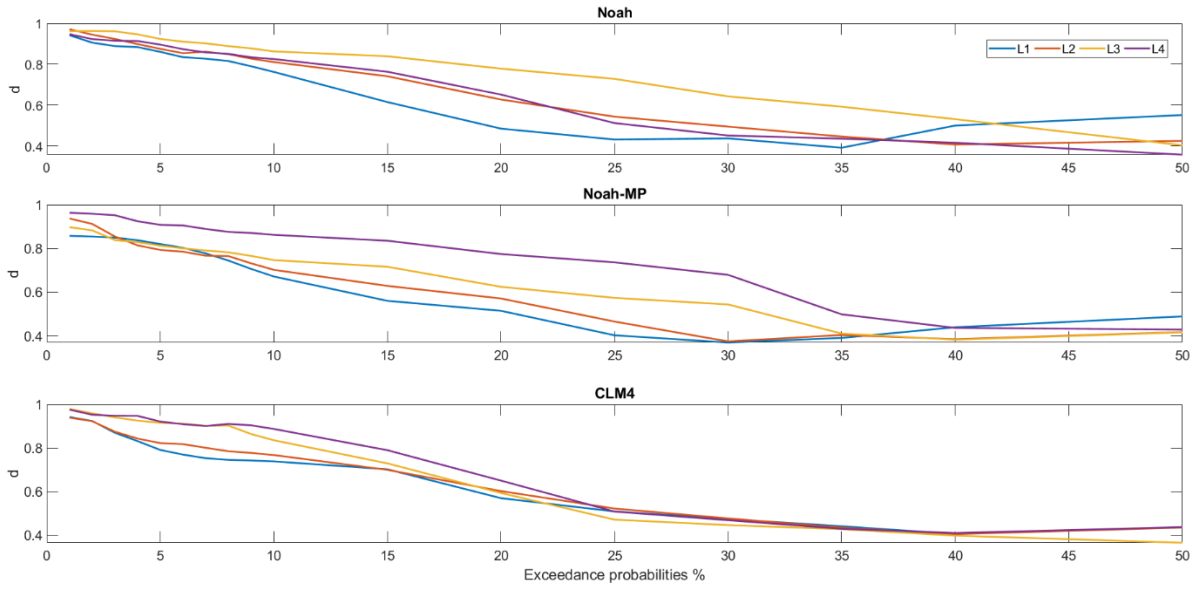


Figure 8. d-scores.

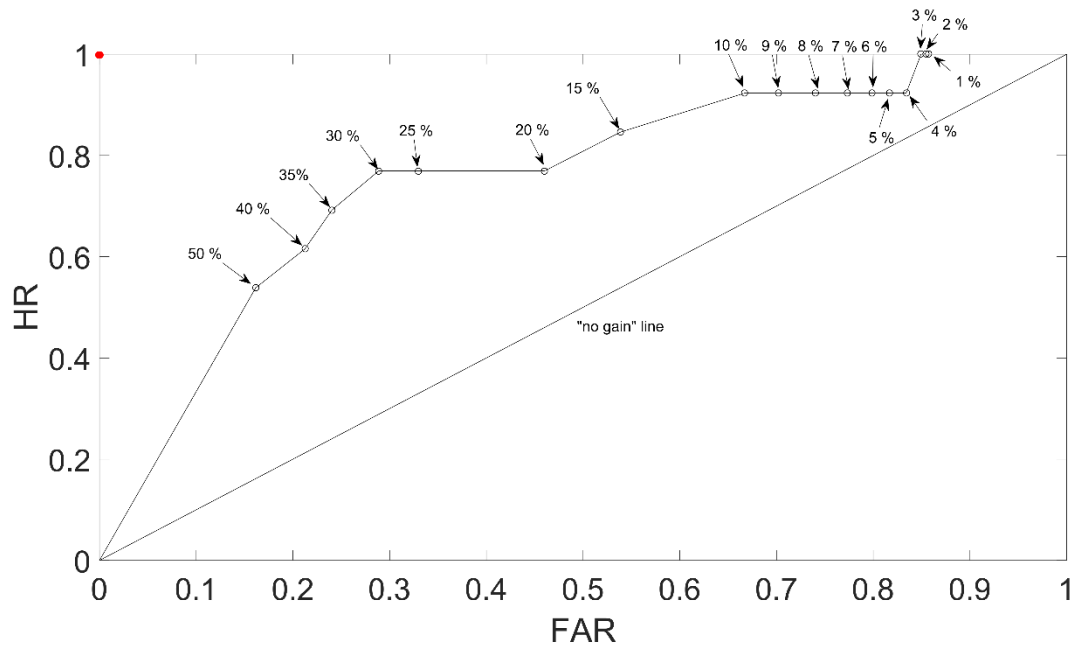


Figure 9. ROC curve for the calculated thresholds using different exceedance probability levels (for Noah-MP at the surface layer). The *no gain* line and the optimal performance point (the red point) are also presented.